DEPARTMENT OF PHYSICS

INELASTIC DARK MATTER: THEORY AND DETECTION PROSPECTS

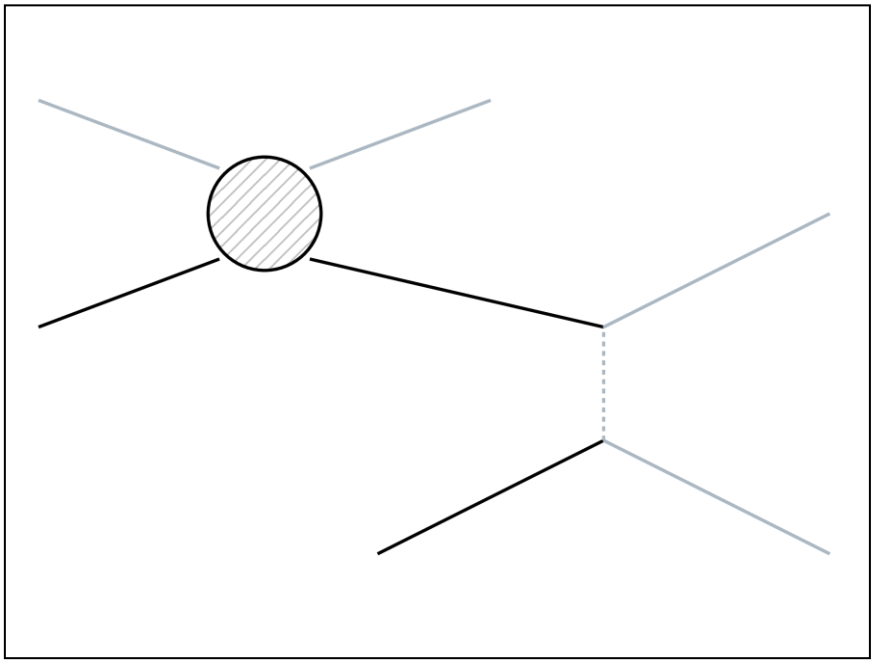

Fredrik Hellström

Degree project for Master of Science (120 HEC) with a major in Physics
2018, 45 HEC
Second Cycle

Master's thesis 2022

Inelastic Dark Matter: Theory and Detection Prospects

FREDRIK HELLSTRÖM

UNIVERSITY OF GOTHENBURG

Department of Physics
University of Gothenburg
Gothenburg, Sweden 2022

Inelastic Dark Matter: Theory and Detection Prospects
FREDRIK HELLSTRÖM
kfuhellstrom@gmail.com

Supervisor: Riccardo Catena, Dpt. of Physics, Chalmers University of Technology
Examiner: Henrik Johannesson, Dpt. of Physics, University of Gothenburg

Department of Physics
Division of Fundamental Physics
University of Gothenburg
SE-412 96 Gothenburg

Cover: Schematic image of a fermionic dark matter particle scattering with a nucleus before pair-annihilating, producing Standard Model fermions. Processes like this are of relevance to neutrino telescopes, as discussed in this thesis.

Typeset in LaTeX
Printed by Humanistens reproservice
Gothenburg, Sweden 2022

Abstract

A wealth of cosmological observations indicate the existence of invisible mass, or dark matter (DM), in the universe. The currently leading hypothesis is that DM consists of as of yet undetected particles with interactions at the weak scale. Weakly interacting DM particles are currently searched for using direct detection experiments, which look for nuclear recoils induced by the non-relativistic scattering of DM particles in low-background detectors, and indirect detection experiments, which search for DM annihilation signals. Neutrino telescopes searching for neutrinos from DM annihilation in the center of the Sun, where DM is expected to be gravitationally captured as a result of DM-nucleus scattering, are an important example of indirect detection experiments.

As of yet, DM has not been definitively detected at any experiment. The absence of such a detection constrains the allowed DM parameter space, and many popular DM candidates are under pressure. A possible explanation for the non-detection is that DM predominantly scatters inelastically with nuclei, implying a mass splitting between the initial and final states of the DM particle. This type of model, called inelastic DM, would be harder to detect with current experiments due to the altered kinematics and has recently attracted a great deal of attention.

In this thesis, I explore the theory and detection prospects of inelastic DM in more generality than has been done before. I calculate the rate at which the Sun captures DM particles, which for the first time is evaluated in the general effective theory of inelastic DM. Using this calculation, I derive novel limits on the coupling coefficients of inelastic DM from the null results of the neutrino telescope IceCube. Furthermore, I calculate corresponding limits from the null results of the direct detection experiments CRESST, PICO and XENON1T. My results show that neutrino telescopes are the most competitive type of detection experiment for part of the parameter space for almost all inelastic DM interaction types. They also provide the insight that neutrino telescopes are indispensable when highly inelastic DM is considered, highlighting an as of yet unexploited complementarity between direct detection experiments and neutrino telescopes.

Contents

1
Introduction

One of the biggest currently unsolved questions in science is the nature and properties of dark matter (DM). A growing number of observations at various scales, ranging all the way from our solar neighborhood to large-scale structure formation and the cosmic microwave background (CMB), indicate that only around 15% of all matter in the universe is composed of the known Standard Model (SM) particles [1]. This normal matter is also-called luminous matter, since it interacts non-negligibly with photons. Little is known about the remaining 85% of matter, but one property it has is that it does not emit light, hence the term DM. Its existence has so far only been inferred from its gravitational interaction with luminous matter, but many experiments, both on Earth and in space, are currently trying to detect other types of interactions. According to most popular DM theories, the existing state-of-the-art detectors and next-generation experiments that are currently under construction have a good chance of detecting DM. However, if a definitive detection continues to elude the global, high-technological search efforts during the coming decade, it may indicate that we are searching for the wrong thing or in the wrong way.

Due to the lack of detailed information regarding the precise nature of DM, many different models regarding its exact properties and interactions exist. The most widely studied category of DM models is the so-called *WIMP* (weakly interacting massive particle), which is expected to have a weak-scale interaction with SM particles and be relatively heavy. In the canonical analysis procedure, two interactions called spin-independent and spin-dependent are considered, as they are in a sense the simplest interactions imaginable. However, a wide array of other types of interactions are both possible and plausible, and have also been studied in recent years. These interactions are described by an *effective field theory* (EFT), which describes the low-velocity behavior of DM-nucleus interactions in a compact way, independently of whatever the high-energy physics details are.

The focus of this thesis is *inelastic* DM. A DM scattering process is called elastic if the initial and final state of the DM particle are the same, and inelastic if the final DM state has a different mass from the initial state. Inelastic DM arises from models where the DM candidate has a low-lying excited state and a subdominant elastic cross section, thereby making processes in which DM is excited or de-excited the dominant form of interaction. Due to the mass splitting between the two DM states, the kinematics of the scattering process becomes very different compared to the elastic case.

Specifically, I will examine the theory of inelastic DM interactions and compute expected event rates at direct and indirect DM detection experiments. Direct detection experiments look for collisions between DM and SM particles, while indirect

detection experiments look for SM particles produced by DM annihilation. Direct detection experiments are typically located deep underground to reduce background. Indirect experiments might be located in space or in lakes or ice on Earth, depending on what kind of signal they search for. Indirect detectors look for DM annihilation signals coming from places where DM is expected to be particularly dense. One such place is the center of the Sun, where DM is expected to amass as a result of being gravitationally captured after losing kinetic energy by scattering with solar nuclei. The indirect detection part of my analysis will focus on neutrino telescope signals from DM annihilation in the solar core.

The results presented in this thesis are new and relevant for current research. I present exclusion limits from neutrino telescope experiments on the DM-nucleon coupling strength for several types of interactions that have previously not been considered in the context of neutrino telescopes. I show that, for most interactions, these limits are the most competitive ones for interesting regions of the parameter space. In addition to this, I present the solar capture rate of DM for the inelastic case of interactions that have previously only been considered for the elastic case.

In the remainder of this chapter, I first give an overview of the cosmological evidence for DM. Then, some theoretically motivated extensions to the SM that predict a DM candidate are briefly presented. Finally, I give a short description of some current experiments that are searching for DM, focusing on the ones included in this thesis.

1.1 Evidence for dark matter

There are several cosmological observations that cannot be explained by only ordinary matter and our current understanding of gravity. At many different scales, discrepancies are found between prediction and observation. Many proposed explanations exist, but the so-called ΛCDM model, where Λ stands for dark energy and CDM for cold DM, explains virtually all of these discrepancies in a satisfactory way. The wide range of phenomena that are explained is the most impressive feature of the DM description, and one that no alternative theory possesses. In this section, some of these discrepancies and the ways in which DM explains them are presented.

1.1.1 Initial predictions and galaxy clusters

The predicted existence of non-luminous matter dates all the way back to 1933 and the Swiss astronomer Fritz Zwicky [2]. He studied the Coma galaxy cluster and estimated its total mass by studying the velocity dispersion of the galaxy cluster and applying the virial theorem to it. The virial theorem relates the average kinetic energy of a stable system to its average potential energy, and from this the total mass of a galaxy cluster can be computed based on the galactic velocities. Zwicky's method resulted in a mass that was two orders of magnitude higher than the result from other methods for estimating the luminous mass. He attributed this discrepancy to a non-luminous matter component that he termed *dunkle Materie*, meaning dark matter. At the time, his results were viewed with much skepticism, due to

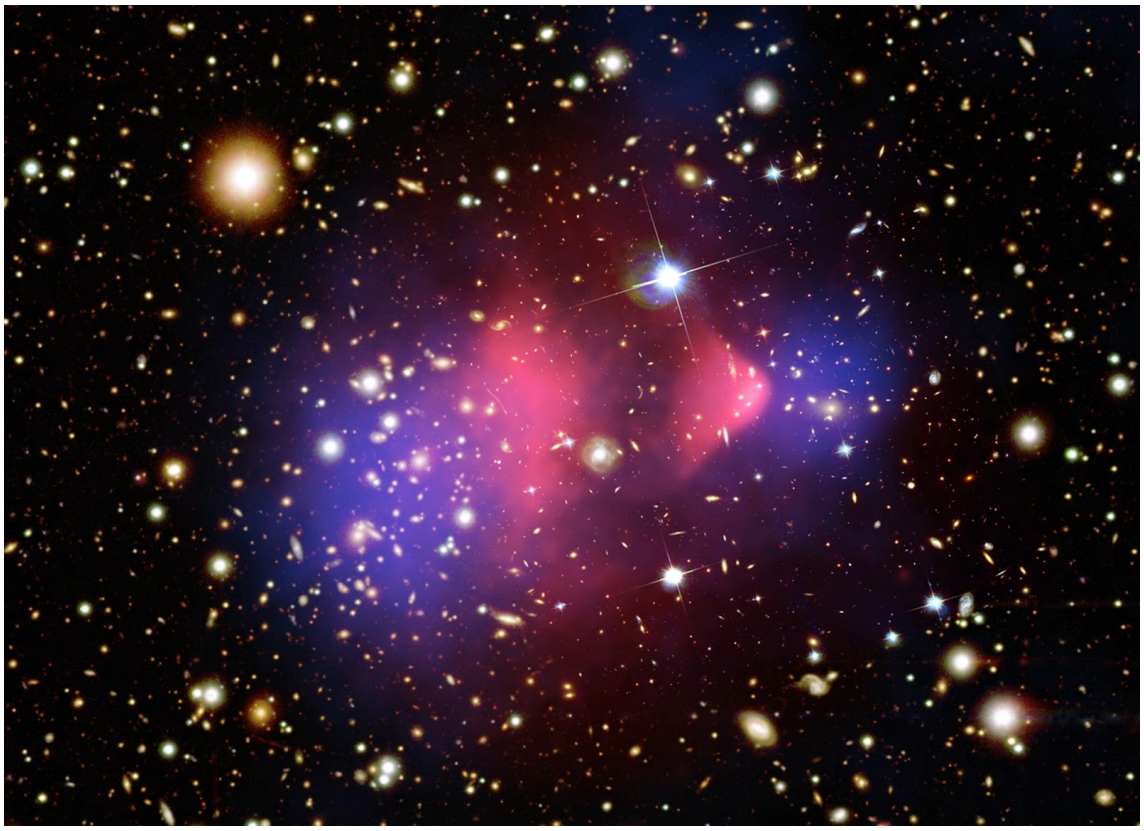

Figure 1.1: An image of the Bullet Cluster, a galaxy cluster collision [4]. In red, the mass centers of normal matter measured with X-rays are illustrated. In blue, the mass centers of total matter measured with gravitational lensing are shown. The discrepancy between these two indicates the existence of DM.

questions regarding the validity of applying the virial theorem to galaxy clusters. Nowadays, the virial theorem is known to apply to most galaxy clusters [1].

Another phenomenon at the scale of galaxy clusters where anomalous observations arise is in the collision of galaxy clusters. In cluster collisions, stars, DM and interstellar gas behave differently from each other. Since the gas interacts electromagnetically, the gas components of the clusters slow down significantly. The stars and DM, in contrast, are almost non-collisional, and are only moderately slowed due to gravitational interaction. To find the distribution of ordinary matter after the collision, X-ray measurements can be used. Most of the ordinary matter in galaxy clusters are in the form of gas, so these measurements find high mass concentrations near the collision center. An independent method that measures the total mass is gravitational lensing, where the bending of light is used as a measure of mass. If the mass concentrations found with this method differ from the X-ray measurements by being further from the collision center, this indicates the existence of non-ordinary matter – DM. A significant example of a galaxy cluster collision is the so-called Bullet Cluster [3]. A graphic illustration of the cluster collision, with the X-ray determined mass concentrations indicated in red and the gravitational lensing ones in blue, is given in figure 1.1. As seen in the figure, the total mass centers and the ordinary mass centers are not coincident. This discrepancy indicates the existence

of DM in the galaxy clusters.

1.1.2 Rotational velocities of spiral galaxies

On the scale of individual galaxies, there are also observations indicating a non-luminous matter component. In the 1970s, astronomer Vera Rubin famously observed a discrepancy between the predicted and measured rotation speeds of stars at the edge of a spiral galaxy [5]. Since the amount of luminous matter contributing to the gravitational force on stars at the edge of a spiral galaxy increases only negligibly beyond a certain point, one expects the rotation speed of stars outside of this point to decrease as a function of the distance from the galactic center. However, Rubin found that the rotation speeds were practically constant all the way out to the galactic rim. One explanation for this is the existence of non-luminous matter, i.e. DM, which contributes to the gravitational force on the galactic edge stars. If DM is distributed in the right way in the galaxy, it can account for the constant rotation speed.

Though DM is the most popular one, there are other proposed explanations for this phenomenon. The most studied alternative is Modified Newtonian Dynamics (MOND) and its relativistic generalization Tensor–vector–scalar gravity (TeVeS) [6, 7], which suggest that we instead need to alter our understanding of gravity and its behavior at large distances. The basic idea is that, for very low accelerations, the relation between force F and acceleration a turns into $F \propto a^2$ instead of $F \propto a$, the typical Newtonian relation. This modification would lead to rotation speeds at the rims of spiral galaxies actually being constant, as is observed. However, a spiral galaxy where the rotation speed actually *does* fall of as predicted by the luminous mass and our current gravity models has recently been discovered [8]. This galaxy is argued to cause a problem for the modified gravity approach. Whereas the DM theory can explain this by saying that the galaxy for some reason is devoid of DM, modified gravity theories have a harder time to adapt to exceptions like this, since they are fine-tuned to describe typical galaxies. Nonetheless, some proponents argue that this observation is still consistent with MOND [9].

1.1.3 Structure formation and the CMB

By studying the early universe, further discrepancies which can be solved by DM are found. One obvious feature of our universe is that there exist structures such as planets, stars, galaxies and galaxy clusters. Explaining why this is the case, rather than everything just being a homogeneous mix of the cosmological ingredients, is not trivial. The current explanation is that, at first, the universe was homogeneous, but small fluctuations arose and eventually grew to form bigger and bigger overdensities, leading to the complex structure that we see today. A problem with this is that, if all matter was ordinary, any inhomogeneities that arose would quickly be wiped out by the radiation that dominated the early universe while they were still small, due to the large interaction between radiation and ordinary matter. If, however, the universe contained a matter component that did not interact much with radiation – DM – inhomogeneities could arise first in DM, and then gravitationally spread to

ordinary matter after growing large enough. In this way, DM is thought to have functioned as an incubator for structure formation [10].

Other DM-related observations come from the cosmic microwave background (CMB). Notoriously discovered by accident in 1964 by Arno Penzias and Robert Wilson [11], the CMB is a snapshot of the early universe that permeates all of space. In the initial stages of the universe, the temperature was too high for atoms to form. Instead, protons and electrons roamed free. Since these particles were charged, they interacted strongly with radiation. Eventually, the universe cooled off, allowing protons and electrons to combine to form hydrogen in an event called recombination. By doing so, they became electrically neutral, significantly lowering their interaction with radiation. The CMB is the remnant of radiation that has traveled through the universe from this point forward, having only barely interacted with anything else ever since. Due to the inhomogeneities required for structure formation, some anisotropies will arise in the CMB. Loosely speaking, the size of these anisotropies are a consequence of the amount of ordinary matter that exists in the universe. Recent measurements of the CMB indicate that no more than around 15% of the matter in the universe can be ordinary, thus predicting a significant DM component in the universe [12].

1.2 Models for dark matter

Many different models for the exact nature of DM exist. Due to the absence of data on non-gravitational interactions between DM and ordinary matter, very few of these specific models have been definitively excluded.

A particle needs to possess a few key properties to be considered a viable DM candidate. Clearly, it needs to have a very weak interaction with ordinary matter. Specifically, it needs to have a very small coupling to the photon, if any, in order for it to be dark. It should also be stable, since it would otherwise decay over time and therefore not be observed today. Furthermore, it should be able to explain structure formation. This requirement sets restrictions on what is called the free streaming length, which is related to how far the particle travels on average between interactions. Typically, one also requires that the current abundance of DM can be explained as a relic from the early universe. For this to happen, DM needs to be in thermal equilibrium with ordinary matter in the early universe, decoupling when the temperature becomes too low. However, alternatives where DM is not thermally produced have also been studied [13, 14].

The term WIMP (weakly interacting massive particle) is frequently used to describe the most studied type of DM candidate. As the name suggests, this category of models has an interaction on the weak scale and is relatively heavy, usually of $O(100)$ GeV or slightly above. These properties are expected since they would give rise to a relic abundance in accordance with what we see today through a thermal production mechanism as discussed above. Similar candidates that are much lighter than this are called light DM (LDM). Other theories predict particles that are much, much heavier, above 10^{10} GeV, which are usually referred to as WIMPzillas. In the following subsections, I give very brief overviews of more specific DM scenarios that can fit into one of these broader categories. If a model can give rise to inelastic DM,

as defined in the beginning of this chapter, this is explicitly mentioned. For further reading on elastic models, see e.g. [15]. For more detailed investigations of inelastic DM models, see [16, 17].

1.2.1 Sterile neutrinos

When trying to come up with a DM candidate, the only reasonable suggestion among the SM particles is the neutrino. It is stable, weakly interacting and has a non-zero mass. However, it falls short when it comes to the free streaming length. Since its mass is so small and interactions so weak, the resulting free streaming length is too long and makes neutrino DM inconsistent with the observed structure formation in the universe. To avoid this problem, a variant of the SM neutrino called the sterile neutrino, with a slightly different interaction and a higher mass, has been proposed as a DM candidate [18, 19].

1.2.2 Supersymmetric WIMPs

In supersymmetry [20], an extension of the SM, all particles are predicted to have so-called superpartners. Supersymmetry states that for each SM fermion, a corresponding boson exists, and for each SM boson, a corresponding fermion exists. One of the main motivations for supersymmetry is to solve the hierarchy problem, which concerns quantum corrections to the Higgs boson mass. The physical masses of particles come from the sum of the bare masses in the Lagrangian plus corrections. The problem with the Higgs mass is that, in the SM, the corrections are on the order of 10^{18} GeV, whereas the physical mass is around 125 GeV. This means that the bare mass also has to be of order 10^{18} GeV, but fine-tuned such that the terms almost precisely cancel to result in the relatively small physical mass that is measured in experiments. This is not impossible, but the fact that the parameters of the theory have to be fine-tuned to such a high accuracy is widely considered a problem. Supersymmetry solves this since the extra superpartners almost cancel the ordinary corrections, thus avoiding the need of fine-tuning.

In supersymmetric theories, the lightest, neutral superpartner (LSP) is a DM candidate [21]. This is due to a symmetry of the theory that makes the lightest superpartner stable. A widely studied candidate is the neutralino. After electroweak symmetry breaking, the neutral higgsinos (superpartners of the Higgs boson) combine with the bino and wino (superpartners of the B and W boson respectively) to form four Majorana fermions called neutralinos. The lightest of these is a good DM candidate, and is one of the most studied WIMP models. If a neutralino consists mainly of only one of the constituent particles, mixing little with the others, it is called higgsino-, bino- or wino-like, depending on which particle contributes most to the neutralino state. If DM consists solely of higgsino-like neutralinos, its mass is estimated to be around 1 TeV [22].

Higgsinos can also give rise to inelastic DM [17]. For higgsino-like DM, the mass splitting between the two lowest neutralino states contains terms of the form m_Z^2/M, where m_Z is the Z boson mass and M is either the bino or wino mass, plus terms of order $O(1/M^2)$. If the bino and wino are very massive, this can lead to a relatively

small $O(100)$ keV mass splitting, possibly detectable by current experiments. This is discussed in more detail in section 2.5.

Other superpartners, like photinos, sneutrinos and gravitinos, can also be DM candidates. The sneutrino has been suggested as an inelastic DM candidate [23].

1.2.3 Axions

Like the DM candidates from supersymmetry, axions [24] are not primarily motivated for their DM properties, but for their ability to solve another problem in particle physics. Their DM candidate status is just an added bonus. Quantum chromodynamics (QCD), the quantum field theory that describes quarks and gluons, is widely successful. However, it has the issue that – unless a parameter is fine-tuned to be very small – it predicts strong violations of charge parity (CP) symmetry, which are not observed in experiment. Similar to the hierarchy problem, it is considered troubling that a parameter has to be very small without any apparent reason. To give a reason for the parameter being small, one can introduce a new symmetry that is spontaneously broken, which can drive the parameter toward zero. This mechanism would also produce a new particle, since all broken symmetries give rise to a boson. The hypothetical new particle from this particular symmetry is called the axion.

The axion is a very light DM candidate. If it were heavy, red giant stars would cool much more rapidly than they are observed to. This process constrains the axion mass to be $\lesssim 10^{-3}$ eV [24].

1.2.4 Other candidates

The array of DM candidates is too wide for an extensive list to be included in this thesis, so I will conclude by very briefly mentioning a few others in addition to those already covered. A candidate from string theory is Kaluza-Klein states [25], where compactified extra dimensions give rise to new particles, the lightest of which is a DM candidate. Another is dark photon DM, where a new, massive boson called a dark photon mediates the interaction between DM and ordinary matter. Dark photon DM can give rise to inelastic DM with $O(100)$ keV mass splittings [17]. Finally, one of the more widely studied inelastic candidates is magnetic inelastic DM [26], where the interaction with SM particles comes from a magnetic dipole operator.

1.3 Dark matter detection experiments

The efforts toward a DM detection using non-gravitational probes are global and have been spanning decades. However, despite the mounting evidence from cosmological observations for its existence, DM has yet to be definitively detected outside of its gravitational presence. There is still hope for a detection in the coming years, since current detectors are reaching incredible sensitivities, which will be improved even further by next-generation experiments that are under construction or in the planning stage. In this section, I give an overview of some of the current experiments

searching for DM, with a special focus on the ones that the results of this thesis are based on.

1.3.1 Direct detection

Direct detection experiments search for nuclear recoils induced by the non-relativistic scattering of Milky Way DM particles in low-background detectors.

Despite the highly advanced technical requirements, the general principle of direct detection experiments is very simple. A detector material is placed in a low background environment and observed. Any scattering event is recorded and analyzed, and if the number of events that look like DM scattering with the detector material exceeds the expected number of background events, it indicates a DM detection. However, due to the extremely weak interaction between DM and ordinary matter, the background needs to be virtually non-existent for a signal to be distinguished. This presents a huge engineering challenge for experimental construction. A few different detector designs exist [27], with more under construction or in the planning phase [28], and their efficiencies in searching for certain DM scenarios differ. Below, a few of the main ones are presented.

1.3.1.1 Noble gas detectors

Noble gas detectors consist of large underground tanks of a low-temperature noble gas in liquid form. An interaction in the detector first generates scintillation light and then frees electrons in the target, giving rise to a second electric signal. Combining the measurement times and intensities of these signals, the position, energy and type of the interaction can be determined. This allows the experiment to separate signal events from background [29].

A big advantage of liquid noble gas detectors is that they are relatively easy to scale up, due to the non-interactive properties of noble gases. The experiment that currently sets the strongest limits on the spin-independent, elastic cross section (and several other interaction types) for all but very small DM masses is XENON1T [30], a ton-scale liquid xenon detector. Its most recent results, which are used in this thesis, were made public in May 2018, based on a run-time of 279 days [31]. Examples of other liquid gas detectors are PandaX [32] and LUX [33].

1.3.1.2 Superheated fluids

Superheated fluid detectors consist of refrigerant fluids kept slightly below their boiling points. When an interaction deposits energy in the target material, a phase transition takes place and a bubble is formed, ready to be detected. In order for an event to be detectable, the bubble formed must be sufficiently large. This automatically removes much of the low-energy background, and is one of the advantages of this type of detector [34].

Some examples of detection experiments using this technique are COUPP [35] and PICO. In this thesis, the PICO-60 run with C_3F_6I from 2013-2014 will be used as it provides the most relevant results for inelastic DM [36]. Later runs of PICO

used C_3F_8, without iodine, making it less sensitive to high mass splittings due to the absence of a high-mass nucleus [37].

1.3.1.3 Cryogenic bolometers

In cryogenic bolometers, the target material is made up of crystals. Detection events cause a phonon signal, which can be recorded. In addition to this, an electric field can be applied over the crystal, giving rise to an electric signal that can be used to distinguish between event types. The selling point for these detectors is that they are able to measure very small recoil energies, thus having increased sensitivity to low-mass DM [38].

Two cryogenic bolometer detectors are CDMS [39] and CRESST. Although newer data from CRESST has been published, the results from CRESST-II will be used in this thesis [40]. The more recent experiment CRESST-III has a smaller exposure and is, in spite of the lowered energy threshold, less relevant than its predecessor for heavy inelastic DM [41]. Despite the focus of CRESST being low-mass DM, its results are competitive when it comes to highly inelastic high-mass DM. The reason for this is that CRESST uses $CaWO_4$ crystals as their target material, and the very high mass of tungsten means that CRESST is sensitive to DM mass splittings that other direct detection experiments cannot reach.

1.3.2 Indirect detection

Indirect detection experiments, as the name implies, do not search for direct interactions between DM and ordinary matter. Instead, they search for SM particles produced by DM annihilation. They do this by looking in the direction of, for example, the centers of our Sun or the Milky Way – places where DM is expected to accumulate due to being gravitationally captured. A more extensive review of indirect detection experiments is given in e.g. [42].

1.3.2.1 Gamma rays

One predicted DM annihilation product is energetic photons called gamma rays. These rays travel virtually undeflected, so if detected they would carry a lot of information on the spatial distribution of DM. This, in combination with an analysis of the gamma ray spectrum, can reveal much about the properties of DM [43].

Since gamma rays would be absorbed in the terrestrial atmosphere, detectors searching for them have to be located in outer space. The most competitive gamma ray detector is the Fermi Large Area Telescope (Fermi-LAT) [44].

1.3.2.2 Cosmic rays

Cosmic rays are high-energetic fluxes of (anti-)protons and nuclei. While ordinary matter cosmic rays are produced by several astrophysical processes, the same is not true for antimatter rays, which can therefore be a low-background DM probe. A drawback of cosmic ray searches is that it is very difficult to determine the origin of the rays, due to the high interaction of the charged rays with other particles.

Examples of cosmic ray DM experiments are PAMELA [45] and the Alpha Magnetic Spectrometer (AMS-02) [46].

1.3.2.3 Neutrino telescopes

Another widely used probe is neutrinos, the spatial origins of which can be easily determined due to their weak interactions with other particles. Since neutrinos are not absorbed in the atmosphere, experiments looking for them can be located on Earth. Neutrino telescopes typically consist of large bodies of water or ice, where Cherenkov light can be produced by interacting neutrinos that pass through the detector [42]. One method of measurement that these experiments use is to search for neutrino-induced muons. While neutrinos interact very weakly, muons couple much more strongly to other particles. Therefore, if a terrestrial detector measures a muon that is going upward, it cannot have traversed through Earth, but has been created by a process at the detector. By accounting for background processes, excess muon measurements can be used as a proxy for the neutrino rate [47]. If the neutrino rate thus computed exceeds the expected background, it may be due to DM annihilation.

Examples of neutrino telescopes are Super-Kamiokande [48] and IceCube. In this thesis, I will use the most recent results on muon fluxes from IceCube [49], as they provide the most relevant indirect detection results for inelastic DM.

1.3.3 Dark matter production

Finally, another way to detect DM is to actually produce it at a particle collider. The DM particles thus produced are not directly measured, but instead inferred by measuring the total energy and momenta of the SM particles that are concurrently produced. If the energy is lower than the initial energy before the collision, one can conclude that the missing energy has escaped as DM particles. The most significant experimental facility that could plausibly produce DM is the Large Hadron Collider (LHC) at CERN. As of yet, no sign of DM has been found at production experiments [50].

2

Theory of Inelastic Dark Matter

Most analyses of dark matter (DM) detection experiments focus on DM that scatters elastically, i.e. the initial and final DM states are the same. However, inelastic scenarios where the final state of the DM particle has a different mass from the initial state have also been widely considered, usually to reconcile experimental results that are in conflict in the elastic case [51, 52]. Due to the mass splitting between the DM states, the kinematics of DM-nucleus scattering is significantly altered. This has a big impact on the results of detection experiments.

In this chapter, the relevant theory for analyzing DM detection experiments from an inelastic perspective is presented and necessary formulas are derived.

2.1 Inelastic kinematics

The DM speed distribution in the Milky Way rest frame is truncated at the galactic escape velocity, which is around 544 km/s [53]. Thus, when we look at DM scattering at either the Sun or Earth, DM will be non-relativistic, even when we take into account the gravitational acceleration and non-zero velocities of the bodies. Therefore, it is sufficient to consider classical, Galilean invariant kinematics. The kinematics of inelastic DM scattering is also discussed in e.g. [17, 54].

The conservation equations that govern the non-relativistic scattering process $\chi N \to \chi^* N$, where χ (χ^*) is the DM ground (excited) state and N is a nuclear state, are, in the nucleus rest frame,

$$\tfrac{1}{2} m_\chi w_i^2 = \tfrac{1}{2} m_N v_N^2 + \tfrac{1}{2} m_{\chi^*} w_f^2 + m_\delta, \tag{2.1}$$

$$m_\chi \vec{w}_i = m_N \vec{v}_N + m_{\chi^*} \vec{w}_f, \tag{2.2}$$

where m_N is the nucleus mass, m_χ and $m_{\chi^*} = m_\chi + m_\delta$ the masses of the DM states, $\vec{v}_N$ the nucleus final velocity, $\vec{w}_i$ ($\vec{w}_f$) the initial (final) DM velocity and m_δ the mass splitting between the DM states.

Squaring the momentum conservation, letting θ be the angle between $\vec{v}_N$ and $\vec{w}_i$, we get

$$\tfrac{1}{2} m_{\chi^*} w_f^2 = \frac{m_\chi^2 w_i^2 + m_N^2 v_N^2 - 2 m_N m_\chi w_i v_N \cos(\theta)}{2 m_{\chi^*}}. \tag{2.3}$$

By using this relation and (2.1), an equation for the nuclear recoil energy $E_R = \frac{1}{2} m_N v_N^2$ can be found, which reads

$$E_R \left(\frac{m_N}{m_{\chi^*}} + 1 \right) - \sqrt{2 m_N E_R} \frac{m_\chi}{m_{\chi^*}} w_i \cos(\theta) + m_\delta - \tfrac{1}{2} m_\chi w_i^2 \frac{m_\delta}{m_{\chi^*}} = 0. \tag{2.4}$$

Turning this into a quadratic equation for E_R, we get

$$E_R^2 + E_R \frac{\mu_*}{m_N}\left(2m_\delta - \frac{m_\chi}{m_{\chi^*}} m_\delta w_i^2 - 2\frac{m_\chi^2}{m_{\chi^*}^2}\cos^2(\theta)\mu_* w_i^2\right) + \\ + m_\delta^2 \frac{\mu_*^2}{m_N^2}\left(1 - \frac{m_\chi}{m_{\chi^*}} w_i^2 + \frac{m_\chi^2}{m_{\chi^*}^2}\frac{w_i^4}{4}\right) = 0, \tag{2.5}$$

where $\mu_* = m_N m_{\chi^*}/(m_N + m_{\chi^*})$ is the reduced mass of the nucleus and DM final state. In the low velocity, low mass splitting limit this equation reduces to

$$E_R^2 + E_R \frac{\mu}{m_N}\left(2m_\delta - 2\mu w_i^2 \cos^2(\theta)\right) + m_\delta^2 \frac{\mu^2}{m_N} = 0, \tag{2.6}$$

where $\mu = m_N m_\chi/(m_N + m_\chi)$. This has maximum and minimum solutions for E_R being

$$E_R^{\max} = \frac{\mu^2}{m_N} w^2 \left(1 + \sqrt{1 - \frac{2m_\delta}{\mu w_i^2}}\right) - \frac{\mu}{m_N} m_\delta, \tag{2.7}$$

$$E_R^{\min} = \frac{\mu^2}{m_N} w^2 \left(1 - \sqrt{1 - \frac{2m_\delta}{\mu w_i^2}}\right) - \frac{\mu}{m_N} m_\delta. \tag{2.8}$$

For these solutions to be real, it is required that

$$w_i \geq w_m = \mathrm{Re}\left\{\sqrt{\frac{2m_\delta}{\mu}}\right\}, \tag{2.9}$$

which translates into the initial center of mass energy being larger than the mass splitting. This is the lowest possible DM speed for scattering to be kinematically allowed.

2.2 Direct detection rates

Direct detection experiments searching for DM try to observe scattering events between ordinary nuclei and DM particles. This is done by having a detector material with a predicted high likelihood to interact with DM in a virtually background free environment. The principles of direct detection are covered in subsection 1.3.1 of this thesis. In this thesis, I will compute event rates and derive limits from the direct detection experiments CRESST [40], PICO [36] and XENON1T [30].

The differential event rate at a direct detection experiment per unit detector mass and unit time is given by [55]

$$\frac{dR}{dE_R} = \sum_T n_T \frac{\rho_\chi}{m_\chi} \int_{w_R}^{\infty} d^3w\, p(\vec{w}) w \frac{d\sigma_T(E_R, w^2)}{dE_R}, \tag{2.10}$$

where the sum runs over all detector nuclei, n_T is the detector material number density, ρ_χ the DM density, m_χ the DM mass, w_R the minimum velocity for which scattering leading to a nuclear recoil energy E_R is possible, $p(\vec{w})$ the DM velocity

distribution and $d\sigma/dE_R$ the differential cross section for DM-nucleus scattering, all evaluated at the detector. To get the total event rate, this is integrated over the intersection of the kinematically allowed recoil energies and the recoil energies that the experiment is sensitive to.

To see how inelasticity affects direct detection results, let us turn to (2.4), which in the low velocity, low mass splitting limit becomes

$$E_R \frac{m_N}{\mu} - w_i \cos(\theta)\sqrt{2m_N E_R} + m_\delta = 0. \tag{2.11}$$

The minimal w_i that solves this equation for a given E_R is

$$w_R = \frac{E_R \frac{m_N}{\mu} + m_\delta}{\sqrt{2m_N E_R}}, \tag{2.12}$$

which itself is minimized with respect to E_R by

$$E_R = \frac{\mu}{m_N} m_\delta, \tag{2.13}$$

for which the minimum speed becomes

$$w_R^{\min} = w_m = \mathrm{Re}\left\{\sqrt{\frac{2m_\delta}{\mu}}\right\}. \tag{2.14}$$

This shows that the velocity space in which scattering is allowed is maximized for a non-zero E_R when $m_\delta > 0$, in contrast to the elastic case. Thus, if DM predominantly scatters elastically with nuclei, we expect the event rate as a function of recoil energy to be featureless (disregarding possible E_R-dependencies in the cross section), whereas in the endothermic inelastic case the spectrum should have a bump. In the exothermic case, where $m_\delta < 0$, the minimum speed is $w_R^{\min} = 0$ as in the elastic case.

2.3 Neutrino telescope rates

Indirect detection experiments search for Standard Model (SM) particles that are produced by DM annihilation. Such experiments can, for example, look for neutrinos originating from places where the DM population is expected to be extra dense, such as at the center of galaxies or celestial objects. In this thesis, I will focus on neutrinos from DM annihilations in the center of the Sun, and derive limits on the DM-nucleon cross section based on results from IceCube [49]. This topic is discussed in e.g. [47].

2.3.1 Solar capture

If DM has a non-zero coupling to quarks, it can be captured by the Sun, a widely studied process [54, 56]. A DM particle is captured if it scatters with a nucleus in the Sun and loses enough energy such that its post-collision speed is below the solar escape velocity. In this section, I compute the rate at which the Sun captures inelastically interacting DM particles as a function of the interaction strength. Although

I explicitly mention the Sun, the general derivation applies to any approximately spherical body. The method I use is based on [56].

First, consider an imaginary surface centered around the Sun at a distance R where the Sun's gravity is negligible. Furthermore, assume that the DM particles at this surface obey an isotropic velocity distribution $p(\vec{u})$, normalized such that

$$\int d^3\vec{u}\, p(\vec{u}) = 1. \tag{2.15}$$

Then, the number of DM particles with velocities that have speeds in the interval $[u, u + du]$ and angles relative to a normal from the Sun in $[\theta, \theta + d\theta]$ in a volume element is given by

$$n_\chi u^2 d\cos\theta du \int_0^{2\pi} d\phi\, p(\vec{u}) = n_\chi 2\pi u^2 p(\vec{u}) d\cos\theta du, \tag{2.16}$$

where n_χ is the DM number density. This can be rewritten in terms of the speed distribution $f(u)$, which for an isotropic velocity distribution is given by $4\pi u^2 p(\vec{u})$, so that

$$n_\chi 2\pi u^2 p(\vec{u}) d\cos\theta du = \tfrac{1}{2} n_\chi f(u) d\cos\theta du. \tag{2.17}$$

The number of particles entering the imaginary surface per unit time is then given by multiplying (2.17) with the velocity perpendicular to the surface, $u\cos\theta$:

$$\tfrac{1}{2} n_\chi f(u) d\cos\theta du \cdot u\cos\theta = \tfrac{1}{4} n_\chi f(u) u du d\cos^2\theta. \tag{2.18}$$

Next, we change variables to angular momentum per mass according to

$$J = Ru\sin\theta, \qquad dJ^2 = -R^2 u^2 d\cos^2\theta. \tag{2.19}$$

Notice that this variable change implies $J \leq Ru$, a requirement that excludes DM particles that do not intersect the surface. The total number of particles entering the surface is (2.18) multiplied by $4\pi R^2$, which in terms of J is

$$\tfrac{1}{4} n_\chi 4\pi R^2 f(u) u du d\cos^2\theta = -\pi n_\chi \frac{f(u)}{u} du dJ^2. \tag{2.20}$$

The minus sign arises since the lower limit of $\cos^2\theta$ corresponds to the upper limit of J^2. Now, consider a spherical shell of the Sun with radius r and thickness $dr \ll r$. Denoting the DM speed at r as w, energy conservation gives us that

$$\tfrac{1}{2} m_\chi u^2 = \tfrac{1}{2} m_\chi w^2 - \frac{G m_\chi M_\odot(r)}{r} = \tfrac{1}{2} m_\chi w^2 - \tfrac{1}{2} m_\chi v^2(r), \tag{2.21}$$

where m_χ is the DM mass, $M_\odot(r)$ the solar mass up to r and $v(r)$ the solar escape velocity at r. From this, we find that $w = \sqrt{u^2 + v^2(r)}$.

Next, we need to know how much time the DM particle spends in the shell. If a particle enters a shell, it also exits it. The perpendicular distance traveled in the

shell is thus $2dr$ and the perpendicular speed is $w\cos\theta$. Therefore, the time spent in the shell is

$$\frac{2dr}{w\cos\theta} = \frac{2dr}{\sqrt{w^2 - w^2\sin^2\theta}} = \frac{2dr}{\sqrt{w^2 - J^2/r^2}}. \tag{2.22}$$

As previously mentioned, the DM particle intersects the shell only if $J \leq rw$. If we introduce $\Omega_v^-(w)$ as the likelihood per unit time that a DM particle of speed w scatters to a speed less than v, the capture rate of the shell can be computed by integrating the inward DM flux (2.20) multiplied by the time spent in the shell (2.22) and $\Omega_v^-(w)$ over J^2, with the upper limit given by r^2w^2. This gives

$$n_\chi \frac{f(u)du}{u} \int_0^{r^2w^2} dJ^2 \frac{2\pi\Omega_v^-(w)dr}{\sqrt{w^2 - J^2/r^2}} = \left(4\pi r^2 dr\right)\, n_\chi \frac{f(u)du}{u} w\Omega_v^-(w). \tag{2.23}$$

Notice that, since $dr \ll r$, the volume of the shell is

$$\frac{4\pi}{3}\left[(r+dr)^3 - r^3\right] \approx 4\pi r^2 dr, \tag{2.24}$$

which is a factor of (2.23). Thus, the capture rate by the Sun per unit volume is, with $n_\chi = \rho_\chi/m_\chi$ where ρ_χ is the DM density,

$$\frac{dC}{dV} = \frac{\rho_\chi}{m_\chi} \int_0^\infty du \frac{f(u)}{u} w\Omega_v^-(w). \tag{2.25}$$

Next, let us study $\Omega_v^-(w)$. I will assume that the solar nuclei are at rest, since for most nuclei the thermal speeds [57] are negligible compared to the DM speeds, which are larger than or equal to the solar escape velocity.

For a DM particle to be captured, its post-collision speed has to be lower than the solar escape velocity $v(r)$, corresponding to an energy of $\frac{1}{2}m_\chi v^2(r)$. Therefore, the recoil energy E_R of the solar nucleus must obey

$$E_R = E_{\chi,i} - E_{\chi,f} - m_\delta \geq \tfrac{1}{2}m_\chi w^2 - \tfrac{1}{2}m_\chi v^2(r) - m_\delta, \tag{2.26}$$

where $E_{\chi,i}$ ($E_{\chi,f}$) is the initial (final) kinetic energy of the DM particle. Thus, since the pre-scattering speed of the DM particle is $w = \sqrt{u^2 + v^2}$, we get

$$E_R \geq E_C = \tfrac{1}{2}mu^2 - m_\delta. \tag{2.27}$$

The kinematics of inelastic scattering was discussed in section 2.1. One of the results relevant for this calculation is the minimum and maximum allowed recoil energies for a given target nucleus, given by

$$E_{R,i}^{\max} = \frac{\mu_i^2}{m_{N,i}} w^2 \left(1 + \sqrt{1 - \frac{2m_\delta}{\mu_i w^2}}\right) - \frac{\mu_i}{m_{N,i}} m_\delta, \tag{2.28}$$

$$E_{R,i}^{\min} = \frac{\mu_i^2}{m_{N,i}} w^2 \left(1 - \sqrt{1 - \frac{2m_\delta}{\mu_i w^2}}\right) - \frac{\mu_i}{m_{N,i}} m_\delta, \tag{2.29}$$

where $m_{N,i}$ is the nucleus mass and μ_i the reduced mass of the nucleus-DM system. Introducing the short-hands $E_L^i = \mathrm{Max}(E_{R,i}^{\min}, E_C)$ and $E_H^i = E_{R,i}^{\max}$ we have

$$E_L^i \geq E_R \geq E_H^i. \tag{2.30}$$

In section 2.1, I also showed that the minimum velocity for scattering to be possible is $w_{m,i} = \mathrm{Re}\left\{\sqrt{\frac{2m_\delta}{\mu_i}}\right\}$. In terms of u, this can be written as

$$u \geq u_{m,i} = \mathrm{Re}\left\{\sqrt{\frac{2m_\delta}{\mu_i} - v^2(r)}\right\}. \tag{2.31}$$

Given these requirements on E_R and u, we can write $\Omega_v^-(w)$ as

$$\Omega_v^-(w) = \sum_i n_i w\, \Theta(u - u_{m,i})\Theta(E_H^i - E_C) \int_{E_L^i}^{E_H^i} dE_R\, \frac{d\sigma(E_R, w^2)}{dE_R}, \tag{2.32}$$

where the sum runs over the most abundant solar nuclei, n_i is the i-th nucleus number density and the Θ's are Heaviside functions which guarantee that capture is kinematically allowed. Notice that n_i is r-dependent, while w, E_H^i and E_L^i all depend on both r and u.

For a more informative expression, we can place restrictions on r and u by inspection of the equality $E_{R,i}^{\max} = E_C$, the point at which the E_R-dependent Heaviside function flips. Explicitly, it reads

$$\frac{\mu_i^2}{m_{N,i}}\left(1 + \sqrt{1 - \frac{2m_\delta}{\mu_i\left(u^2 + v^2(r)\right)}}\right) - \frac{\mu_i}{m_{N,i}} m_\delta = \tfrac{1}{2} m u^2 - m_\delta. \tag{2.33}$$

This equality has two positive solutions for u,

$$u_{\pm,i}^C = \frac{\sqrt{2m_\chi m_{N,i} v(r)}}{|m_\chi - m_{N,i}|}\sqrt{1 + \delta\frac{m_{N,i} - m_\chi}{m_\chi v^2(r)} \pm \sqrt{1 + 2\delta\frac{m_{N,i} - m_\chi}{m_{N,i} m_\chi v^2(r)}}}. \tag{2.34}$$

Since E_C is real for all u, $E_C > E_{R,i}^{\max}$ for sufficiently large u and $E_{R,i}^{\min}$ and $E_{R,i}^{\max}$ form a parabola, E_C crosses them either twice or not at all. If the solutions in (2.34) are real, it crosses twice, meaning that part of the parameter space allows for capture. For the solutions to be real, the escape velocity $v(r)$ must fulfill the inequality

$$v(r) \geq v_{L,i} = \mathrm{Re}\left\{\sqrt{\frac{2m_\delta\left(m_\chi - m_{N,i}\right)}{m_\chi m_{N,i}}}\right\}. \tag{2.35}$$

Since $v(r)$ is a monotonically decreasing function, it has an inverse $v^{-1}(v)$ and

$$r \leq r_{L,i} = v^{-1}(v_{L,i}), \tag{2.36}$$

where $r_{L,i} = r_\odot$ if $v_{L,i} < v(r_\odot)$, where $r_\odot$ is the solar radius, and $r_{L,i} = 0$ if capture by the Sun is impossible, i.e. $v_{L,i} > v(0)$. For light nuclei, this is very restrictive, making hydrogen a non-captor even for small positive mass splittings.

Finally, the u parameter space that can contribute to capture is bounded below by $u_{m,i}$, the minimum speed for scattering to be possible, and bounded above by $u_+^{C,i}$. It is possible that $E_C > E_{R,i}^{\max}$ for $u_{m,i} \leq u \leq u_-^{C,i}$, in which case this region does not contribute to capture.

Next, we consider the speed distribution, $f(u)$. In the Standard Halo Model [53], DM particles in the galactic rest frame are assumed to follow a Maxwell-Boltzmann velocity distribution $p_0(\vec{u})$ given by

$$p_0(\vec{u}) = N_0 \exp\left(-\frac{3}{2v_D^2}u^2\right), \tag{2.37}$$

where v_D is a dispersion velocity taken to be 270 km/s and N_0 is a constant which normalizes the integral of the velocity distribution to 1. Since the Sun moves with a speed v_S with respect to the galactic rest frame, we need to make the transformation $\vec{u} \to \vec{u} + \vec{v}_S$. To obtain the speed distribution, we also integrate over the solid angle and multiply by u^2. This yields, with θ being the angle between $\vec{u}$ and $\vec{v}_s$,

$$\begin{aligned} f(u) &= N_0\, u^2 \exp\left[-\frac{3}{2v_D^2}\left(u^2 + v_S^2\right)\right] \int d\Omega\, \exp\left(-\frac{3}{v_D^2} u\, v_S \cos\theta\right) \\ &= \frac{N_0 v_D^2}{3\, v_S}\, u \left[\exp\left(-\frac{3}{2v_D^2}\left(u - v_S\right)^2\right) - \exp\left(-\frac{3}{2v_D^2}\left(u + v_S\right)^2\right)\right]. \end{aligned} \tag{2.38}$$

We now have all the ingredients of the capture rate. To get the total rate, we integrate (2.25) over the Sun's volume to obtain

$$C = \frac{\rho_\chi}{m_\chi} \sum_i \int_0^{r_{L,i}} dr 4\pi r^2 n_i(r) \int_{u_{m,i}(r)}^{u_+^{C,i}(r)} du \frac{f(u)}{u} w\, \Theta(E_H^i - E_c) \int_{E_L^i(u,r)}^{E_H^i(u,r)} dE_R \frac{d\sigma(w^2, E_R)}{dE_R}. \tag{2.39}$$

Note that the integration limits and Heaviside function in this expression depend on both m_χ and m_δ.

2.3.2 Solar thermalization of dark matter

In the previous section, the capture rate of DM is computed. Indirect detection experiments like IceCube search for products of DM annihilation in the Sun, and one typically assumes that capture and annihilation are in equilibrium so that the annihilation rate is half of the capture rate. However, this assumption relies on the ability of DM to thermalize in the Sun through repeated scattering shedding its kinetic energy. For elastic scattering, even very small cross sections enable thermalization, a subject that has been extensively studied both analytically and numerically [58, 59]. A conservative lower limit for the required elastic cross section is $\sigma_e \gtrsim 10^{-49}$ cm^2 [17]. For inelastic scattering, an issue is that the inelastic kinematics is very restrictive at low DM energies, and thus may severely slow down or completely prohibit the thermalization process.

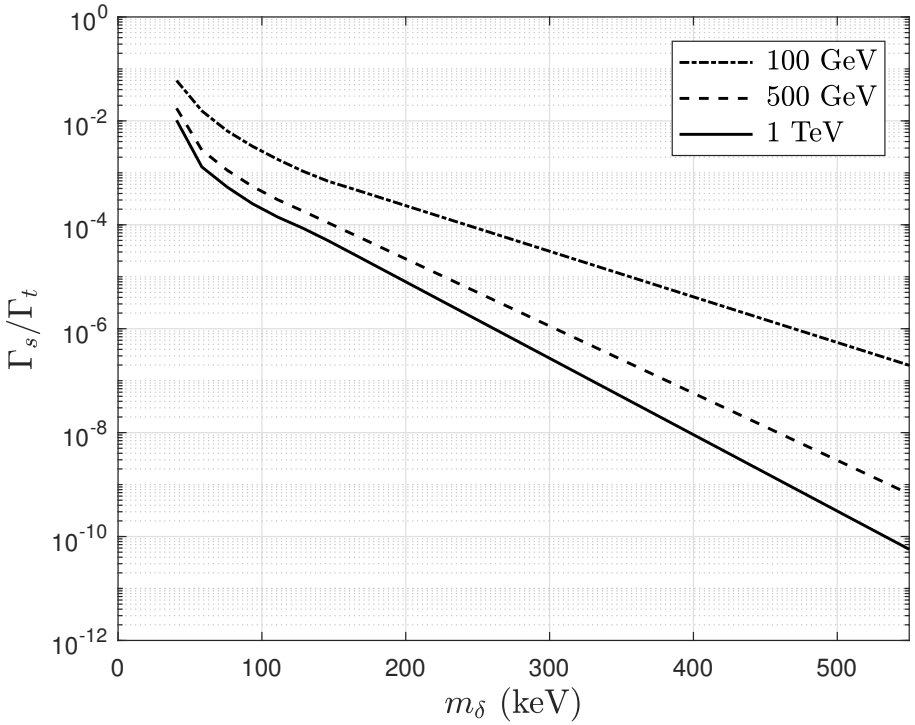

Figure 2.1: Suppression of the annihilation signal Γ_s relative to the equilibrium case Γ_t as computed in [62]. For mass splittings above 200 keV and masses above 500 GeV, exponential extrapolation in mass splitting and mass has been used.

When studying inelastic capture, it is common to assume that a subdominant elastic process is strong enough to allow thermalization, but weak enough to be negligible for capture and direct detection experiments [60, 61]. Attempts to obtain even stronger results have made hand-wavy order-of-magnitude arguments that suggest that even in the absence of an elastic process, inelastic DM thermalizes. However, a recent paper [62] presented detailed Monte-Carlo simulations of the thermalization process for inelastic DM. The results show that DM thermalizes only for very small mass splittings in the absence of elastic scattering, making the actual annihilation highly suppressed compared to the thermalized annihilation. Based on these results, I will later illustrate neutrino telescope limits both for an unsuppressed annihilation rate and a weaker suppressed one. The two cases correspond to having a big enough subdominant elastic cross section to thermalize and not having any elastic interaction, respectively.

Since [62] computed the suppression only for m_χ up to 500 GeV and m_δ up to 200 keV, I have to extrapolate the results in both of these parameters when deriving limits outside of this parameter space. In both of these parameters, I do exponential extrapolation. In order to make my limits as conservative as possible, I base my suppression functions on the scenario with an inelastic cross section of 10^{-45} cm^2. For any model with a larger cross section, the actual suppression is therefore lower than what I use. The suppressions that are used when computing limits are shown in figure 2.1. As seen in the figure, the potential effect of this suppression can be

highly significant, reaching a relative suppression of around $5 \cdot 10^{-11}$ for a 1 TeV mass and 550 keV mass splitting.

2.3.3 Annihilation and muon flux

After accumulating in the Sun, DM can begin to pairwise annihilate if the density is high enough. This annihilation is expected to give rise to SM particles that can be observed at indirect detection experiments. In this section, I will compute the expected muon flux at neutrino telescopes given a solar capture rate under the assumption of equilibrium, largely following [47].

The number of DM particles N in the Sun changes according to the separable differential equation

$$\frac{dN}{dt} = C - E \cdot N(t) - A \cdot N^2(t), \tag{2.40}$$

where C is the capture rate while E and A are constants related to the evaporation and annihilation rates. Under the assumption of negligible evaporation, which is fair for both elastic and inelastic scenarios [62], the solution with $N(0) = 0$ is

$$N = \sqrt{\frac{C}{A}} \tanh\Big(\sqrt{CA}\, t\Big). \tag{2.41}$$

The annihilation rate is given by $\Gamma = \frac{1}{2} A N^2$, which using (2.41) can be written as

$$\Gamma(t) = \frac{C}{2} \tanh^2\left(\frac{t}{\tau}\right), \qquad \tau \equiv 1/\sqrt{CA}, \tag{2.42}$$

where τ is an equilibration time. If $t \gg \tau$, we find that $\Gamma = C/2$, the equilibrium solution. As discussed in the previous section, this is an excellent approximation if there is a sufficiently strong elastic DM-nucleon scattering process. However, it is invalid for purely inelastic scenarios with mass splittings bigger than a few keV. The equilibrium solution can however be straightforwardly adjusted to account for this by multiplying with the suppression factor described in the previous section.

Given this DM annihilation rate, the expected neutrino-induced muon rate in a terrestrial detector like IceCube can be computed, given some model assumptions. If we denote the different DM annihilation branching ratios that give rise to neutrinos as B_χ^f where f is the final state, the differential neutrino flux reaching the detector is

$$\frac{dN_\nu}{dE_\nu} = \frac{\Gamma}{4\pi D^2} \sum_f B_\chi^f \frac{dN_\nu^f}{dE_\nu}, \tag{2.43}$$

where D is the distance from the Sun's core to the detector and dN_ν^f the branched differential neutrino rates. This neutrino flux gives rise to a muon flux, which can formally be written as

$$\frac{dN_\mu}{dE_\mu} = N_A \int_{E_\mu}^{\text{th}} dE_\nu \int_0^\infty d\lambda \int_{E_\mu}^{E_\nu} dE'_\mu P(E_\mu, E'_\mu; \lambda) \frac{d\sigma_\nu(E_\nu, E'_\mu)}{dE'_\mu} \frac{dN_\nu}{dE_\nu}, \tag{2.44}$$

where E_ν the neutrino energy, E'_μ the initial muon energy, $d\sigma_\nu/dE'_\mu$ the differential cross section for an E_ν neutrino producing a E'_μ muon, λ the muon range in the medium, $P(E_\mu, E'_\mu; \lambda)$ the probability that the E'_μ muon will have an energy E_μ after traveling a length λ in the detector, N_A the detector nucleon density and E_μ^{th} the threshold energy of the detector.

All of these computations are implemented in the DarkSUSY Fortran package [63, 64], which I use for computing the muon fluxes.

2.4 Effective theory of dark matter-nucleus interactions

When computing event rates at detection experiments, the DM-nucleus cross section is an important parameter. Many studies just assume the cross section to be constant in order to simplify the analysis. Another method of calculating it is to consider a specific extension of the SM that includes a DM candidate and compute the cross section for the relevant interaction. This method is appropriate if the goal is to constrain a certain model.

However, in recent years a model-independent approach has become more common. It exploits the non-relativistic nature of DM-nucleus scattering to construct an effective theory, which is valid in the low-velocity regime. Effective operators can either be constructed from the top by taking the non-relativistic limit of relativistic operators in a given particle physics theory and integrating out the high-energy details, or by starting from the bottom by simply writing down all of the allowed low-velocity operators. In this section, I present a method of constructing an effective theory describing all possible interactions between DM and nuclei from the ground up, originally developed in [65] and later generalized to the case of inelastic scattering in [52].

In the low velocity limit, the requirement of Lorentz invariance turns into Galilean invariance. The Galilean invariant quantities from which we can build operators are the particle spins $\vec{S}_\chi$ and $\vec{S}_N$, their relative velocity $\vec{v}$ and the momentum transfer $\vec{q}$ in the scattering. Based on these quantities, we can form the Hermitian invariant operators

$$\mathbb{1}, \qquad \frac{\hat{q}}{m_N}, \qquad \hat{v}_\perp, \qquad \hat{S}_\chi, \qquad \hat{S}_N, \tag{2.45}$$

where m_N is the nucleon mass and the perpendicular velocity $\vec{v}_\perp$ is given by

$$\vec{v}_\perp = \vec{v} + \left(\frac{1}{2\mu} + \frac{m_\delta}{q^2}\right)\vec{q}, \tag{2.46}$$

where μ is the reduced DM-nucleon mass and m_δ the DM mass splitting. The name $\vec{v}_\perp$ is motivated by the fact that $\vec{v}_\perp \cdot \vec{q} = 0$. Note that the addition of the m_δ-dependent term to $\vec{v}_\perp$ is the only non-kinematic difference between elastic and inelastic scattering as described in the effective theory [52].

Next, in order to facilitate studies of nuclear responses, we want to separate the the perpendicular velocity as $\hat{v}_\perp = \hat{v}_\perp^T + \hat{v}_\perp^N$, where the two terms capture the

$$
\begin{aligned}
\hat{O}_1 &= \mathbb{1} & \hat{O}_9 &= \hat{S}_\chi \cdot \left(\hat{S}_N \times \tfrac{\hat{q}}{m_N}\right) \\
\hat{O}_3 &= \hat{S}_N \cdot \left(\tfrac{\hat{q}}{m_N} \times \hat{v}_\perp\right) & \hat{O}_{10} &= \hat{S}_N \cdot \tfrac{\hat{q}}{m_N} \\
\hat{O}_4 &= \hat{S}_\chi \cdot \hat{S}_N & \hat{O}_{11} &= \hat{S}_\chi \cdot \tfrac{\hat{q}}{m_N} \\
\hat{O}_5 &= \hat{S}_\chi \cdot \left(\tfrac{\hat{q}}{m_N} \times \hat{v}_\perp\right) & \hat{O}_{12} &= \hat{S}_\chi \cdot \left(\hat{S}_N \times \hat{v}_\perp\right) \\
\hat{O}_6 &= \left(\hat{S}_\chi \cdot \tfrac{\hat{q}}{m_N}\right)\left(\hat{S}_N \cdot \tfrac{\hat{q}}{m_N}\right) & \hat{O}_{13} &= \left(\hat{S}_\chi \cdot \hat{v}_\perp\right)\left(\hat{S}_N \cdot \tfrac{\hat{q}}{m_N}\right) \\
\hat{O}_7 &= \hat{S}_N \cdot \hat{v}_\perp & \hat{O}_{14} &= \left(\hat{S}_\chi \cdot \tfrac{\hat{q}}{m_N}\right)\left(\hat{S}_N \cdot \hat{v}_\perp\right) \\
\hat{O}_8 &= \hat{S}_\chi \cdot \hat{v}_\perp & \hat{O}_{15} &= -\left(\hat{S}_\chi \cdot \tfrac{\hat{q}}{m_N}\right)\left[\left(\hat{S}_N \times \hat{v}_\perp\right) \cdot \tfrac{\hat{q}}{m_N}\right]
\end{aligned}
$$

Table 2.1: List of the fourteen possible effective operators for a DM-nucleon interaction mediated by a heavy particle of at most spin 1.

nucleus center of mass and the nucleon motion relative to the nucleus respectively. Furthermore, we rewrite the spatial quantities as coordinate space operators. This can be done using momentum operators, according to

$$\hat{q} = -i\overleftarrow{\nabla}_x \delta\left(\vec{x} - \vec{y} + \vec{r}\right) - i\delta\left(\vec{x} - \vec{y} + \vec{r}\right)\overrightarrow{\nabla}_x, \tag{2.47}$$

$$\hat{v}_\perp^T = \delta\left(\vec{x} - \vec{y} + \vec{r}\right)\left(\frac{i\overrightarrow{\nabla}_x}{m_\chi} - \frac{i\overrightarrow{\nabla}_y}{m_T}\right) + \frac{\hat{q}}{2\mu}, \tag{2.48}$$

$$\hat{v}_\perp^N = \frac{1}{2m_N}\left(i\overleftarrow{\nabla}_r \delta\left(\vec{r} - \vec{r}_i\right) - i\delta\left(\vec{r} - \vec{r}_i\right)\overrightarrow{\nabla}_r\right), \tag{2.49}$$

where $\overleftrightarrow{\nabla}_a$ with a right-arrow (left-arrow) acts on the $\vec{a}$-coordinate of the corresponding wave-function of the initial (final) state, $\vec{x}$ is the nucleus center of mass position, $\vec{y}$ the DM position, $\vec{r}$ the nucleon position in the nucleus center of mass frame and m_T the nucleus mass.

Now, we want to construct the possible quantum interaction operators that can be formed from these operators, with the restriction that the mediating particle is heavy and of at most spin 1. These restrictions mean that only contact operators that are at most linear in $\hat{S}_\chi$, $\hat{S}_N$ and $\hat{v}_\perp$ are included. With this, 14 linearly independent operators can be written. The possible operators are given in table 2.1. For historical reasons, no operator is labeled $\hat{O}_2$.

Next, we want to write down a Hamiltonian density describing the DM-nucleus interaction, assuming that DM interacts with nucleons through one-body interactions only. The most general such Hamiltonian density that can be written is a linear combination of the fourteen operators, with different couplings to protons and neutrons, summed over all constituent nucleons. In terms of isoscalar and isovector coupling constants, this can be written as

$$\mathcal{H}(\vec{r}) = \sum_{i=1}^{A}\sum_{\tau=0}^{1}\sum_{k=1}^{15} c_k^\tau \hat{O}_k^{(i)}(\vec{r}) t_{(i)}^\tau, \tag{2.50}$$

where $t^0 = \mathbb{1}$ and $t^1 = \sigma_3$, the third Pauli matrix. Note that $c_2^\tau = 0$, due to the operator numbering convention.

We now want to rewrite this Hamiltonian density using the coordinate space

operators given in (2.47-2.49). As it turns out, it can be written as

$$\begin{aligned}\mathcal{H}(\vec{r}) = \sum_{\tau=0}^{1}\sum_{i=1}^{A}\Bigg[&\hat{l}_0^\tau\delta\left(\vec{r}-\vec{r}_i\right) + \hat{l}_{0A}^\tau\frac{1}{2m_N}\left(i\overleftarrow{\nabla}_r\cdot\vec{\sigma}(i)\delta\left(\vec{r}-\vec{r}_i\right) - i\delta\left(\vec{r}-\vec{r}_i\right)\vec{\sigma}(i)\cdot\overrightarrow{\nabla}_r\right)\\ &\hat{l}_5^\tau\cdot\vec{\sigma}\delta\left(\vec{r}-\vec{r}_i\right) + \hat{l}_M^\tau\cdot\frac{1}{2m_N}\left(i\overleftarrow{\nabla}_r\delta\left(\vec{r}-\vec{r}_i\right) - i\delta\left(\vec{r}-\vec{r}_i\right)\overrightarrow{\nabla}_r\right)\\ &\hat{l}_E^\tau\cdot\frac{1}{2m_N}\left(\overleftarrow{\nabla}_r\times\vec{\sigma}(i)\delta\left(\vec{r}-\vec{r}_i\right) + \delta\left(\vec{r}-\vec{r}_i\right)\vec{\sigma}\times\overleftarrow{\nabla}_r\right)\Bigg]t_{(i)}^\tau,\end{aligned} \tag{2.51}$$

where the coefficients $\hat{l}_i^\tau$ are given by

$$\begin{aligned}\hat{l}_0^\tau =& c_1^\tau + i\left(\frac{\hat{q}}{m_N}\times\hat{v}_T^\perp\right)\cdot\hat{S}_\chi c_5^\tau + \hat{v}_T^\perp\cdot\hat{S}_\chi c_8^\tau + i\frac{\hat{q}}{m_N}\cdot\hat{S}_\chi c_{11}^\tau,\\ \hat{l}_{0A}^\tau =& -\tfrac{1}{2}\left(c_7^\tau + i\frac{\hat{q}}{m_N}\cdot\hat{S}_\chi c_{14}^\tau\right),\\ \hat{l}_5^\tau =& \tfrac{1}{2}\Bigg(i\frac{\hat{q}}{m_N}\times\hat{v}_T^\perp c_3^\tau + \hat{S}_\chi c_4^\tau + \frac{\hat{q}}{m_N}\frac{\hat{q}}{m_N}\cdot\hat{S}_\chi c_6^\tau + \hat{v}_T^\perp c_7^\tau + i\frac{\hat{q}}{m_N}\times\hat{S}_\chi c_9^\tau + i\frac{\hat{q}}{m_N}c_{10}^\tau\\ &+ \hat{v}_T^\perp\times\hat{S}_\chi c_{12}^\tau + i\frac{\hat{q}}{m_N}\hat{v}_T^\perp\cdot\hat{S}_\chi c_{13}^\tau + i\hat{v}_T^\perp\frac{\hat{q}}{m_N}\cdot\hat{S}_\chi c_{14}^\tau + \frac{\hat{q}}{m_N}\times\hat{v}_T^\perp\frac{\hat{q}}{m_N}\cdot\hat{S}_\chi c_{15}^\tau\Bigg),\\ \hat{l}_M^\tau =& i\frac{\hat{q}}{m_N}\times\hat{S}_\chi c_5^\tau - \hat{S}_\chi c_8^\tau,\\ \hat{l}_E^\tau =& \tfrac{1}{2}\left(\frac{\hat{q}}{m_N}c_3^\tau + i\hat{S}_\chi c_{12}^\tau - \frac{\hat{q}}{m_N}\times\hat{S}_\chi c_{13}^\tau - i\frac{\hat{q}}{m_N}\frac{\hat{q}}{m_N}\cdot\hat{S}_\chi c_{15}^\tau\right).\end{aligned} \tag{2.52}$$

To illustrate how the coefficients l are obtained, consider the operator $\hat{O}_{12}$. It can be rewritten according to

$$\begin{aligned}\hat{O}_{12} &= \hat{S}_\chi\left(\hat{S}_N\times\hat{v}_\perp\right)\rightarrow\delta(\vec{r}-\vec{r}_i)\hat{S}_\chi\cdot\left[\vec{\sigma}\times\left(\hat{v}_\perp^T+\hat{v}_\perp^N\right)\right] \\ &= \left(\hat{v}_\perp^T\times\hat{S}_\chi\right)\cdot\vec{\sigma}\delta(\vec{r}-\vec{r}_i) + i\hat{S}_\chi\cdot\left(\overleftarrow{\nabla}_r\times\vec{\sigma}(i)\delta\left(\vec{r}-\vec{r}_i\right) + \delta\left(\vec{r}-\vec{r}_i\right)\vec{\sigma}\times\overleftarrow{\nabla}_r\right),\end{aligned} \tag{2.53}$$

from which it follows that $\hat{l}_5^\tau$ should contain $\hat{v}_\perp^T\times\hat{S}_\chi c_{12}^\tau$ and $\hat{l}_E^\tau$ should contain $ic_{12}^\tau\hat{S}_\chi$. Repeating this process for all operators yields (2.52). To obtain the full Hamiltonian, all that is left is to integrate (2.51) over all space, which is easily done using the delta functions.

Now, our final goal is to compute a differential cross section, as this is necessary to compute event rates at experiments. The differential cross section is obtained by folding the matrix element with the invariant phase space, which after some manipulation gives the expression [66]

$$\frac{d\sigma}{dE_R} = \frac{m_T}{32\pi w^2 m_\chi^2 m_N^2}\left[\frac{1}{2j_\chi+1}\frac{1}{2j_N+1}\sum_{\text{spins}}|\mathcal{M}|^2\right], \tag{2.54}$$

where m_T is the target nucleus mass and $\mathcal{M}$ the Galilean invariant matrix element.

The matrix elements needed for the above expression can be computed from the Hamiltonian H according to

$$i\mathcal{M}(2\pi)^3\delta(\vec{p}_f-\vec{p}_i) = \langle f|H|i\rangle, \tag{2.55}$$

where i and f are the initial and final states of the DM-nucleus system and $\vec{p}_i$ and $\vec{p}_f$ the corresponding total momenta. Next, the products of operators and plane waves in (2.51) are expanded in spherical harmonics and vector spherical harmonics and the matrix element is squared, initial spins being averaged over and final spins summed over. Skipping the details of this involved calculation, which are covered at length in e.g. [66, 67], the result can be written in the relatively compact form (given some simplifying assumptions about the nuclear wave-functions)

$$\begin{aligned}
&\frac{1}{(2j_\chi+1)}\frac{1}{(2j_N+1)}\sum_{\text{spins}}|\mathcal{M}|^2 = \frac{4\pi}{2j_N+1}\sum_{\tau=0}^{1}\sum_{\tau'=0}^{1}\\
&\left\{\left[R_M^{\tau\tau'}\left(v_\perp^T,\tfrac{q^2}{m_N^2}\right)W_M^{\tau\tau'}(y)+R_{\Sigma''}^{\tau\tau'}\left(v_\perp^T,\tfrac{q^2}{m_N^2}\right)W_{\Sigma''}^{\tau\tau'}(y)+R_{\Sigma'}^{\tau\tau'}\left(v_\perp^T,\tfrac{q^2}{m_N^2}\right)W_{\Sigma'}^{\tau\tau'}(y)\right]\right.\\
&+\frac{q^2}{m_N^2}\left[R_{\Phi''}^{\tau\tau'}\left(v_\perp^T,\tfrac{q^2}{m_N^2}\right)W_{\Phi''}^{\tau\tau'}(y)+R_{\Phi''M}^{\tau\tau'}\left(v_\perp^T,\tfrac{q^2}{m_N^2}\right)W_{\Phi''M}^{\tau\tau'}(y)\right.\\
&\left.\left.+R_{\Phi'}^{\tau\tau'}\left(v_\perp^T,\tfrac{q^2}{m_N^2}\right)W_{\Phi'}^{\tau\tau'}(y)+R_{\Delta}^{\tau\tau'}\left(v_\perp^T,\tfrac{q^2}{m_N^2}\right)W_{\Delta}^{\tau\tau'}(y)+R_{\Delta\Sigma'}^{\tau\tau'}\left(v_\perp^T,\tfrac{q^2}{m_N^2}\right)W_{\Delta\Sigma'}^{\tau\tau'}(y)\right]\right\},
\end{aligned} \tag{2.56}$$

where j_χ and j_N are the DM and nucleus spins respectively. In this expression, the $W^{\tau\tau'}$ are nuclear response functions evaluated within the nuclear shell model with the harmonic oscillator as the underlying single-particle basis, depending on $y=(qb/2)^2$ where b is the harmonic oscillator size parameter. The $R^{\tau\tau'}$ are DM response functions, explicitly given by

$$R_M^{\tau\tau'}\left(v_\perp^T,\tfrac{q^2}{m_N^2}\right)=c_1^\tau c_1^{\tau'}+\frac{j_\chi(j_\chi+1)}{3}\frac{q^2}{m_N^2}\left(v_T^{\perp 2}c_5^\tau c_5^{\tau'}+v_T^{\perp 2}c_8^\tau c_8^{\tau'}+c_{11}^\tau c_{11}^{\tau'}\right), \tag{2.57}$$

$$R_{\Phi''}^{\tau\tau'}\left(v_\perp^T,\tfrac{q^2}{m_N^2}\right)=\frac{q^2}{4m_N^2}c_3^\tau c_3^{\tau'}+\frac{j_\chi(j_\chi+1)}{12}\left(c_{12}^\tau-\frac{q^2}{m_N^2}c_{15}^\tau\right)\left(c_{12}^{\tau'}-\frac{q^2}{m_N^2}c_{15}^{\tau'}\right), \tag{2.58}$$

$$R_{\Phi''M}^{\tau\tau'}\left(v_\perp^T,\tfrac{q^2}{m_N^2}\right)=c_3^\tau c_1^{\tau'}+\frac{j_\chi(j_\chi+1)}{3}\left(c_{12}^\tau-\frac{q^2}{m_N^2}c_{15}^\tau\right)c_{11}^{\tau'}, \tag{2.59}$$

$$R_{\Phi'}^{\tau\tau'}\left(v_\perp^T,\tfrac{q^2}{m_N^2}\right)=\frac{j_\chi(j_\chi+1)}{12}\left(c_{12}^\tau c_{12}^{\tau'}+\frac{q^2}{m_N^2}c_{13}^\tau c_{13}^{\tau'}\right), \tag{2.60}$$

$$\begin{aligned}
R_{\Sigma''}^{\tau\tau'}\left(v_\perp^T,\tfrac{q^2}{m_N^2}\right)=&\frac{q^2}{m_N^2}c_{10}^\tau c_{10}^{\tau'}+\frac{j_\chi(j_\chi+1)}{12}\left[c_4^\tau c_4^{\tau'}+\frac{q^2}{m_N^2}\left(c_4^\tau c_6^{\tau'}+c_6^{\tau'}c_4^\tau\right)\right.\\
&\left.+\frac{q^4}{m_N^2}c_6^\tau c_6^{\tau'}+v_T^{\perp 2}c_{12}^\tau c_{12}^{\tau'}+\frac{q^2}{m_N^2}v_T^{\perp 2}c_{13}^\tau c_{13}^{\tau'}\right],
\end{aligned} \tag{2.61}$$

$$\begin{aligned}
R_{\Sigma'}^{\tau\tau'}\left(v_\perp^T,\tfrac{q^2}{m_N^2}\right)=&\frac{v_T^{\perp 2}}{8}\left(\frac{q^2}{m_N^2}c_3^\tau c_3^{\tau'}+c_7^\tau c_7^{\tau'}\right)\frac{j_\chi(j_\chi+1)}{12}\left[c_4^\tau c_4^{\tau'}+\frac{q^2}{m_N^2}c_9^\tau c_9^{\tau'}\right.\\
&\left.+\frac{v_T^{\perp 2}}{2}\left(c_{12}^\tau-\frac{q^2}{m_N^2}c_{15}^\tau\right)\left(c_{12}^{\tau'}-\frac{q^2}{m_N^2}c_{15}^{\tau'}\right)+\frac{q^2}{2m_N^2}v_T^{\perp 2}c_{14}^\tau c_{14}^{\tau'}\right],
\end{aligned} \tag{2.62}$$

$$R_{\Delta}^{\tau\tau'}\left(v_\perp^T,\tfrac{q^2}{m_N^2}\right)=\frac{j_\chi(j_\chi+1)}{3}\left(\frac{q^2}{m_N^2}c_5^\tau c_5^{\tau'}+c_8^\tau c_8^{\tau'}\right), \tag{2.63}$$

$$R_{\Delta\Sigma'}^{\tau\tau'}\left(v_\perp^T,\tfrac{q^2}{m_N^2}\right)=\frac{j_\chi(j_\chi+1)}{3}\left(c_5^\tau c_4^{\tau'}-c_8^\tau c_9^{\tau'}\right), \tag{2.64}$$

so the c_i^τ coefficients determine the DM response functions, which in turn determine what nuclear response functions will be activated in the interaction. For example, if only one of the coefficients c_1, c_5, c_8 or c_{11} is non-zero, the nuclear response will consist only of $W_M^{\tau\tau'}$. This operator corresponds to the typically assumed standard nuclear response, usually computed with the Helm form factor [27]. Therefore, for the operators $\hat{O}_1$, $\hat{O}_5$, $\hat{O}_8$ and $\hat{O}_{11}$ the Helm form factor is an adequate approximation for the detailed shell model form factors.

2.5 Inelastic dark matter from supersymmetry

In this section, I give a very brief introduction to supersymmetry, presenting little more than the minimal amount of material required to arrive at some relevant properties of nearly pure Higgsino DM. The purpose of this section is to provide some particle physics background illustrating an example of why the parameter space of DM-nucleon interactions examined in this thesis is relevant. It is not necessary for an interpretation of the results of the thesis, and can be skipped entirely. More complete introductions to supersymmetry are given in e.g. [68] or [20], upon which much of this section is based.

First, the Wess-Zumino model is introduced as a simple context to discuss supersymmetry transformations. Then, a general recipe for constructing a supersymmetric model with supersymmetry breaking terms is given. After this, the recipe is applied to the MSSM (Minimal Supersymmetric Model), and the possibility of neutralino DM is considered. Finally, some remarks on what requirements need to be fulfilled for nearly pure higgsino DM to be a thermal relic detectable at current experiments are made.

2.5.1 A general supersymmetric model

The general idea behind supersymmetry is that every fermion has a superpartner, i.e. a boson that has all the same quantum numbers except for spin, and vice versa. This symmetry between fermions and bosons is called supersymmetry. The simplest model that can realize this symmetry is the free, massless Wess-Zumino model, consisting of a Weyl fermion ψ_α (where α is a spinor index), a complex scalar field ϕ with spin 0 and an auxiliary scalar field F, where ψ and ϕ are each other's superpartners. The reason for introducing the auxiliary field is that before enforcing the equations of motion, the fermion ψ has four real degrees of freedom, while the complex scalar field ϕ only has two. Thus, for the number of fermionic and bosonic degrees of freedom to match, an additional complex scalar field needs to be introduced. The object containing ψ_α, ϕ and F is called a chiral supermultiplet.

The Lagrangian of this theory is, with $\bar{\sigma}^\mu = (\mathbb{1}, -\vec{\sigma})$ where $\vec{\sigma}$ are the Pauli matrices,

$$\mathcal{L}_f = -\partial_\mu \phi^* \partial^\mu \phi + i\bar{\psi}_\alpha \bar{\sigma}^\mu \partial_\mu \psi^\alpha + F^* F, \tag{2.65}$$

containing only the kinetic terms of the fields. Note that this gives the equation of motion $F = 0$ for the auxiliary field, thus making it vanish on-shell. The supersymmetry transformations relating the superpartners can then be written as, with

ϵ being an infinitesimal anti-commuting Weyl fermion object,

$$\begin{aligned}\delta\phi &= \epsilon^\alpha \psi_\alpha, \\ \delta\psi_\alpha &= -i\sigma^\mu \epsilon^\dagger_\alpha \partial_\mu \phi + \epsilon_\alpha F, \\ \delta F &= -i\epsilon^\dagger_\alpha \bar{\sigma^\mu} \partial_\mu \psi^\alpha. \end{aligned} \tag{2.66}$$

These transformations leave the Lagrangian (2.65) invariant. Note that in the absence of F, these transformations are the simplest ones transforming the fermion into the scalar and vice-versa without changing the Lagrangian. Going forward, the spinor indices α will be suppressed.

To show that supersymmetry is a valid symmetry, one also needs to show that the associated operators form a group. To show closure under the symmetry, a necessary condition, we can compute the action of a commutator of two supersymmetry transformations, $[\delta_1, \delta_2]X$, where X is any of the fields. The result is

$$[\delta_1, \delta_2]X = i(\epsilon_1 \sigma^\mu \epsilon_2^\dagger + \epsilon_2 \sigma^\mu \epsilon_1^\dagger)\partial_\mu X, \tag{2.67}$$

the momentum operator. The momentum operator is the generator of Poincare symmetry, another symmetry of the theory, showing that the symmetry is closed. The fact that supersymmetry transformations generate Poincare symmetry in this way is the basis of supergravity (SUGRA) theories, where local supersymmetry generates general relativity.

Now that the free Wess-Zumino model has been constructed, the next step is to add interactions. We will add an index i to the fields, to allow for many supermultiplets. For a Lagrangian to be renormalizable, its terms need to be of at most dimension 4. Looking at (2.65), the dimensions of ϕ, ψ and F are, respectively, 1, $\frac{3}{2}$ and 2. With this, the only terms we can write that fulfill this requirement and are invariant under supersymmetry are

$$\mathcal{L}_i = -\tfrac{1}{2} W^{ij} \psi_i \psi_j + W^i F_i + \text{h.c.}, \tag{2.68}$$

where h.c. indicates the hermitian conjugate of the explicit terms. Here, W^{ij} and W^i are polynomials in ϕ and ϕ^* of degrees 1 and 2, respectively. Since the free Lagrangian $\mathcal{L}_f$ was invariant on its own, so must the interacting Lagrangian $\mathcal{L}_i$. There can be no term depending only on ϕ and ϕ^*, since by the supersymmetry transformations (2.66) such a term would be linear in ψ without derivatives or F, and can therefore not be canceled by any other term in $\mathcal{L}_i$. Quadratic terms in F_i are likewise excluded, since they too cannot be canceled by any other term in $\mathcal{L}_i$.

To study the W-polynomials, we apply the supersymmetry transformations to (2.68). This yields

$$\begin{aligned}\delta\mathcal{L}_i = &-\frac{1}{2}\frac{\partial W^{ij}}{\partial \phi_k}\epsilon\psi_k\psi_i\psi_j - \frac{1}{2}\frac{\partial W^{ij}}{\partial \phi^{*k}}\epsilon^\dagger\psi^\dagger k\psi_i\psi_j + iW^{ij}\partial_\mu\phi_j\psi_i\sigma^\mu\epsilon^\dagger - W^{ij}\psi_i\epsilon F_j \\ &+ iW^i\partial_\mu\psi_i\sigma^\mu\epsilon^\dagger + \frac{\partial W^j}{\partial\phi_i}\psi_i\epsilon F_j + \text{h.c.}\end{aligned} \tag{2.69}$$

The first row of this equation immediately comes from the variation of the W^{ij}-term, and the second row from the W^i-term, by use of the identity $-\epsilon^\dagger\bar{\sigma}^\mu\partial_\mu\psi = \partial_\mu\psi\sigma^\mu\epsilon^\dagger$.

The first two terms cannot cancel against anything else in (2.69). The second term vanishes only if $\frac{\partial W^{ij}}{\partial \phi^{*k}}$ does, so W^{ij} must not depend on ϕ^{*k}. For the first term to vanish, the Fierz identity can be used, which implies that

$$\epsilon\psi_i\psi_j\psi_k + \epsilon\psi_j\psi_k\psi_i + \epsilon\psi_k\psi_i\psi_j = 0, \tag{2.70}$$

so if $\frac{\partial W^{ij}}{\partial \phi_k}$ is totally symmetric in i, j and k, the term does vanish. By these conditions, and the fact that W^{ij} is a linear polynomial in ϕ_i, we can write

$$W^{ij} = M^{ij} + y^{ijk}\phi_k = \tfrac{\partial^2 W}{\partial\phi_i\partial\phi_j}, \qquad W \equiv \tfrac{1}{2}M^{ij}\phi_i\phi_j + \tfrac{1}{6}y^{ijk}\phi_i\phi_j\phi_k, \tag{2.71}$$

where W is called the superpotential. The physical interpretations of the coefficients M^{ij} and y^{ijk} are a fermionic mass matrix and a Yukawa coupling between a scalar and two fermions, respectively.

For the fourth and sixth terms in (2.69) (the ones linear in F_j) to cancel, it is necessary that $W^{ij} = \frac{\partial W^j}{\partial \phi_i}$, so that

$$W^i = \tfrac{\partial W}{\partial \phi_i} = M^{ij}\phi_j + \tfrac{1}{2}y^{ijk}\phi_j\phi_k, \tag{2.72}$$

relating W^i to the superpotential as well. This condition is actually sufficient for the third and fifth term to be written as a total derivative, which vanishes upon integration of the Lagrangian density. Using the definitions of W^i and W^{ij},

$$\partial_\mu W^i = \partial_\mu\left(M^{ij}\phi_j + \tfrac{1}{2}y^{ijk}\phi_j\phi_k\right) = M^{ij}\partial_\mu\phi_j + y^{ijk}\phi_k\partial_\mu\phi_j = W^{ij}\partial_\mu\phi_j, \tag{2.73}$$

so that the relevant terms in the variation of the Lagrangian can be written

$$iW^{ij}\partial_\mu\phi_j\psi_i\sigma^\mu\epsilon^\dagger + iW^i\partial_\mu\psi_i\sigma^\mu\epsilon^\dagger = \partial_\mu\left(iW^i\psi_i\sigma^\mu\epsilon^\dagger\right), \tag{2.74}$$

which vanishes upon integration.

Now, looking at the F-part of the full Lagrangian, $F_iF^{*i} + W^iF_i + W_i^*F^{*i}$, the equation of motion for F is now $F_i = -W_i^*$. Making this replacement in the full Lagrangian $\mathcal{L}_f + \mathcal{L}_i$, using the explicit forms of W^{ij} and W^i, we get

$$\begin{aligned}\mathcal{L}_c = &-\partial_\mu\phi^*\partial^\mu\phi + i\bar{\psi}_\alpha\bar{\sigma}^\mu\partial_\mu\psi^\alpha - V_c(\phi,\phi^*) - \\ &\left(\tfrac{1}{2}M^{ij}\psi_i\psi_j + \tfrac{1}{2}y^{ijk}\phi_i\psi_j\psi_k + \text{h.c.}\right),\end{aligned} \tag{2.75}$$

where $V_c(\phi,\phi^*) = W^kW_k^* = F^{*k}F_k$ is the scalar potential of the theory given by

$$\begin{aligned}V_c(\phi,\phi^*) = &M_{ik}^*M^{kj}\phi^{*i}\phi_j + \tfrac{1}{2}M^{in}y_{jkn}^*\phi_i\phi^{*j}\phi^{*k} + \\ &\tfrac{1}{2}M_{in}^*y^{jkn}\phi^{*i}\phi_j\phi_k + \tfrac{1}{4}y^{ijn}y_{kln}^*\phi_i\phi_j\phi^{*k}\phi^{*l}.\end{aligned} \tag{2.76}$$

With this, the theory of a collection of chiral supermultiplets is fully specified by its kinetic terms and the superpotential W.

The next step is to allow for gauge interactions. To this end, we need to introduce the gauge supermultiplet, consisting of a spin 1 massless gauge boson field A_μ^a (where a is a gauge group index), a two-component Weyl fermion λ^a, the superpartner of A_μ^a, and an auxiliary real bosonic field D^a. Similar to the chiral supermultiplet case, the

auxiliary field is needed to preserve supersymmetry off-shell. Off-shell, λ^a has four real degrees of freedom, whereas A^a_μ only has three, since one is removed by gauge invariance. On-shell, the equations of motion remove two and one degrees of freedom respectively, such that both fields have two remaining. Including the auxiliary field D^a adds one off-shell bosonic degree of freedom that vanishes on-shell.

Under gauge transformations, the fields change according to

$$\begin{aligned} A^a_\mu &\to A^a_\mu + \partial_\mu \Lambda^a + g f^{abc} A^b_\mu \Lambda^c, \\ \lambda^a &\to \lambda^a + g f^{abc} \lambda^b \Lambda^c, \\ D^a &\to D^a + g f^{abc} D^b \Lambda^c, \end{aligned} \tag{2.77}$$

where Λ^a is an infinitesimal parameter, g a coupling constant and f^{abc} the structure constants of the gauge group. In the ordinary way, one can thus write down the Lagrangian

$$\mathcal{L}_g = -\tfrac{1}{4} F^a_{\mu\nu} F^{\mu\nu a} + i\lambda^{\dagger a} \bar{\sigma}^\mu \nabla_\mu \lambda^a + \tfrac{1}{2} D^a D^a, \tag{2.78}$$

where $F^a_{\mu\nu}$ and ∇_μ are the field strength and covariant derivative respectively, defined as

$$F^a_{\mu\nu} \equiv \partial_\mu A^a_\nu - \partial_\nu A^a_\mu + g f^{abc} A^b_\mu A^c_\nu, \qquad \nabla_\mu \lambda^a \equiv \partial_\mu \lambda^a + g f^{abc} A^b_\mu \lambda^c. \tag{2.79}$$

To show that this is a supersymmetric theory, we need to find the supersymmetry transformations. They turn out to be

$$\begin{aligned} \delta A^a_\mu &= -\tfrac{1}{\sqrt{2}} \lambda^{\dagger a} \bar{\sigma}_\mu \epsilon + \text{h.c.}, \\ \delta \lambda^a &= \tfrac{i}{2\sqrt{2}} \sigma^\mu \bar{\sigma}^\nu \epsilon F^a_{\mu\nu} + \frac{1}{\sqrt{2}} \epsilon D^a, \\ \delta D^a &= \tfrac{i}{\sqrt{2}} \nabla_\mu \lambda^{\dagger a} \bar{\sigma}_\mu \epsilon + \text{h.c.}, \end{aligned} \tag{2.80}$$

where ϵ is an infinitesimal Weyl fermion parameter of the symmetry. Just as for the chiral supermultiplet case, it can be shown that the commutator of two supersymmetry transformations gives the momentum operator,

$$[\delta_1, \delta_2] X = i(-\epsilon_1 \sigma^\mu \epsilon_2^\dagger + \epsilon_2 \sigma^\mu \epsilon_1^\dagger) \nabla_\mu X, \tag{2.81}$$

where X is any of the fields A^a_μ, λ^a or D^a.

To allow for interactions between the chiral and gauge multiplets, we first need to specify how the chiral supermultiplets transform under the gauge group. The gauge and supersymmetry transformations commute, so all fields in the same chiral supermultiplet need to transform the same under the gauge group. Therefore, with X_i being one of the fields in the i-th chiral supermultiplet,

$$X_i \to X_i + i g \Lambda^a T^a X_i, \tag{2.82}$$

with g and Λ^a defined as before and T^a being a matrix in the representation of the gauge group that the supermultiplet transforms under. As is familiar from the

SM, the derivatives ∂_μ in the Lagrangian (2.75) need to be replaced with covariant derivatives ∇_μ for the action to be gauge-invariant, with

$$\nabla_\mu X_i = \partial_\mu \phi_i - igA^a_\mu T^a X_i. \tag{2.83}$$

This substitution automatically adds interactions between the chiral supermultiplet fields and the gauge boson field A^a_μ. However, interactions with λ^a and D^a need to be added manually. Their dimensions are, from looking at (2.78), $\frac{3}{2}$ and 2 respectively, so the terms with dimension of at most 4 are (with coefficients such that the Lagrangian is supersymmetric)

$$\mathcal{L}_e = g\phi^* T^a \phi D^a - \sqrt{2}g(\phi^* T^a \psi \lambda^a + \text{h.c.}). \tag{2.84}$$

To complete the combination of the gauge and chiral supermultiplets, the supersymmetry transformations of the chiral supermultiplet fields need to be changed. The derivatives need to become covariant derivatives, and δF_i needs an extra term, so that the transformations become

$$\begin{aligned}
\delta\phi_i &= \epsilon\psi_i, \\
\delta\psi_i &= -i\sigma^\mu \epsilon^\dagger \nabla_\mu \phi_i + \epsilon_\alpha F_i, \\
\delta F_i &= -i\epsilon^\dagger \bar{\sigma}^\mu \nabla_\mu \psi_i + \sqrt{2}gT^a \phi_i \epsilon^\dagger \lambda^{\dagger a},
\end{aligned} \tag{2.85}$$

The D^a part of the Lagrangian is $\frac{1}{2}D^a D^a + g\phi^* T^a \phi D^a$. As for the F_i fields, this yields an equation of motion $D^a = -g\phi^* T^a \phi$ that allow us to replace D^a with the scalar fields. The scalar potential (2.76) thus changes to become

$$V(\phi, \phi^*) = F^{*i}F_i + \tfrac{1}{2}D_a D^a = V_c(\phi, \phi^*) + \tfrac{1}{2}g_a^2(\phi^* T^a \phi)^2, \tag{2.86}$$

where the two different contributions are called F-terms and D-terms respectively. The full Lagrangian of this general supersymmetric theory is the sum of (2.75) with covariant derivatives, (2.78) and (2.84), explicitly

$$\begin{aligned}
\mathcal{L} = &\quad \mathcal{L}_c^{\text{cov}} + \mathcal{L}_g + \mathcal{L}_e \\
= &- \partial_\mu \phi^* \partial^\mu \phi + i\bar{\psi}_\alpha \bar{\sigma}^\mu \partial_\mu \psi^\alpha - \left(\tfrac{1}{2}M^{ij}\psi_i\psi_j + \tfrac{1}{2}y^{ijk}\phi_i\psi_j\psi_k + \text{h.c.}\right) \\
&- \tfrac{1}{4}F^a_{\mu\nu}F^{\mu\nu a} + i\lambda^{\dagger a}\bar{\sigma}^\mu \nabla_\mu \lambda^a + \tfrac{1}{2}D^a D^a + g\phi^* T^a \phi D^a \\
&- \sqrt{2}g(\phi^* T^a \psi \lambda^a + \text{h.c.}) - V(\phi, \phi^*).
\end{aligned} \tag{2.87}$$

This, combined with (2.86), is a general recipe that we will use when we consider the MSSM.

The model considered thus far has an exact supersymmetry. For any theory that attempts to describe nature, this cannot be the case, since it would imply that all superpartners have the same mass. Due to the fact that no superpartner to any of the SM particles has been found yet, supersymmetry must be broken, if it exists. Many different models for supersymmetry breaking exist, but in practice it is sufficient to simply add supersymmetry breaking terms with coupling constants of positive mass-dimension to the Lagrangian. This is referred to as soft supersymmetry breaking, and is in fact an effective theory induced by proper, spontaneous supersymmetry

breaking [20]. For a general supersymmetric theory, the possible soft supersymmetry breaking terms are

$$\mathcal{L}_s = -\left(\tfrac{1}{2}M_a\lambda^a\lambda^a + \tfrac{1}{6}a^{ijk}\phi_i\phi_j\phi_k + \tfrac{1}{2}b^{ij}\phi_i\phi_j + t^i\phi_i + \text{h.c.}\right) - \left(m^2\right)^i_j\phi^{j*}\phi_i, \quad (2.88)$$

where some of the terms may be forbidden depending on the gauge symmetries.

2.5.2 The MSSM and neutralino dark matter

In the previous subsection, we found a general recipe for a supersymmetric theory with soft supersymmetry breaking terms. This can now be applied to the Minimal Supersymmetric Model (MSSM), by constructing chiral and gauge supermultiplets containing the SM particles. All that is needed to fully specify the theory is to write down the superpotential W_M and the soft supersymmetry breaking terms.

The superpotential can be constructed from the scalar field parts of the chiral supermultiplets. All of the SM fermions are in chiral supermultiplets, as are the scalar Higgs fields. In the MSSM, there are actually two Higgs doublets, labeled H_u and H_d, rather than just the one in the SM. One reason for this is that not all quarks would get masses otherwise [20]. The labels of the different Higgs doublets label what kind of quarks they give masses to.

The superpotential of the MSSM is, following (2.71),

$$W^{(M)} = \tilde{\bar{u}}\mathbf{y_u}\tilde{Q}H_u - \tilde{\bar{d}}\mathbf{y_d}\tilde{Q}H_d - \tilde{\bar{e}}\mathbf{y_e}\tilde{L}H_d + \mu H_u H_d, \quad (2.89)$$

where $\tilde{Q}$ are the superpartners of the right-handed quarks, $\tilde{\bar{u}}$ of the left-handed up-type quarks, $\tilde{\bar{d}}$ of the left-handed down-type quarks, $\tilde{\bar{L}}$ of the left-handed leptons, $\tilde{\bar{e}}$ the right-handed leptons, $\mathbf{y_u}$, $\mathbf{y_d}$ and $\mathbf{y_e}$ 3×3 Yukawa coupling matrices, and μ a Higgs mass parameter. The quark superpartners are called squarks and the lepton superpartners are called sleptons. In principle, more terms are allowed in the superpotential than I have written here. However, they violate either baryon or lepton number conservation, and would (among other things) imply a finite proton life-time, much shorter than current experimental constraints allow. To get rid of these terms, the MSSM includes a symmetry called R-parity, defined by the operator

$$P_R = (-1)^{3(B-L)+2s}, \quad (2.90)$$

where B is the baryon number, L the lepton number and s the spin. All SM particles have eigenvalue $+1$ under this operator, whereas their superpartners have -1. Thus, this symmetry prevents SM particles from decaying into superpartners and vice versa. An implication of this is that the lightest supersymmetric particle (LSP) cannot decay into an SM particle, thereby making it stable.

The soft supersymmetry breaking terms are, following (2.88),

$$\begin{aligned}\mathcal{L}_s^{(M)} = &-\tfrac{1}{2}\left(M_3\tilde{g}\tilde{g} + M_2\tilde{W}\tilde{W} + M_1\tilde{B}\tilde{B} + \text{h.c.}\right)\\ &-\left(\tilde{\bar{u}}\mathbf{a_u}\tilde{Q}H_u - \tilde{\bar{d}}\mathbf{a_d}\tilde{Q}H_d - \tilde{\bar{e}}\mathbf{a_e}\tilde{L}H_d + \text{h.c.}\right)\\ &-\tilde{Q}^\dagger\mathbf{m_Q^2}\tilde{Q} - \tilde{L}^\dagger\mathbf{m_L^2}\tilde{L} - \tilde{\bar{u}}\mathbf{u_{\bar{u}}^2}\tilde{\bar{u}}^\dagger - \tilde{\bar{d}}\mathbf{m_{\bar{d}}^2}\tilde{\bar{d}}^\dagger - \tilde{\bar{e}}\mathbf{m_{\bar{e}}^2}\tilde{\bar{e}}^\dagger\\ &-m_{H_u}^2H_u^*H_u - m_{H_d}^2H_d^*H_d - (bH_uH_d + \text{h.c.}),\end{aligned} \quad (2.91)$$

where $\tilde{g}$, $\tilde{W}$ and $\tilde{B}$ are the superpartners of the gluon (gluino), W boson (wino) and B boson (bino) respectively, and the M_i are the corresponding mass parameters. The $\mathbf{a_i}$ and $\mathbf{m_i^2}$ are 3×3 matrices with dimensions mass and mass squared respectively, and m_i^2 and b are parameters of dimension mass squared.

The supersymmetry breaking terms give mass terms to the bino and neutral wino. These particles are not the physical ones that are expected to be observable in nature, but they mix with the two higgsinos $\tilde{H}_d^0$ and $\tilde{H}_u^0$ (superpartners of the two Higgs bosons) to form four mass eigenstates called neutralinos, denoted $\tilde{N}_0$ to $\tilde{N}_3$. If a neutralino is the LSP (and it probably is [22]), it is a viable DM candidate: it is electrically neutral, massive, stable on cosmological time-scales and interacts weakly with ordinary matter.

To see what the neutralino states look like, we need to diagonalize their mass matrix. To find the mass matrix, we define a vector $\psi = (\tilde{B}, \tilde{W}^0, \tilde{H}_d^0, \tilde{H}_u^0)^T$ containing the neutral gaugino gauge eigenstates. The matrix will then have M_1 and M_2 from (2.91) on the diagonal, $-\mu$ from (2.89) on the higgsino off-diagonal and terms of the form gv_i mixing higgsinos, binos and winos, stemming from (2.84). The v_i, where $i \in u, d$, are the Higgs vacuum expectation values (VEVs). A description of how the Higgs bosons acquire their VEVs in the MSSM is given in [20]. The mass terms are then $-\frac{1}{2}\psi^0 M_{\tilde{N}} \psi^{0T} + \text{h.c.}$ where the mass matrix is

$$M_{\tilde{N}} = \begin{pmatrix} M_1 & 0 & -g'v_d/\sqrt{2} & g'v_u/\sqrt{2} \\ 0 & M_2 & gv_d/\sqrt{2} & -gv_u/\sqrt{2} \\ -g'v_d/\sqrt{2} & gv_d/\sqrt{2} & 0 & -\mu \\ g'v_u/\sqrt{2} & -gv_u/\sqrt{2} & -\mu & 0 \end{pmatrix}. \tag{2.92}$$

This will give rise to physical masses that are the square-roots of the eigenvalues of $M_{\tilde{N}} M_{\tilde{N}}^\dagger$, the lightest of which corresponds to a possible DM candidate (given that no charged superpartner is lighter).

2.5.3 Nearly pure higgsino dark matter

We now want to restrict ourselves to a particular neutralino DM scenario that is phenomenologically relevant for the results presented in this thesis, specifically nearly pure inelastic higgsino DM.

Working in the limit where the electroweak symmetry breaking effects are a small perturbation to the neutralino mass matrix ($m_Z \ll |\mu + M_1|, |\mu + M_2|$ with m_Z being the Z boson mass) the neutralino mass eigenstates mix very little, nearly being the pure gauge eigenstates. In this limit, the eigenvalues of $M_{\tilde{N}} M_{\tilde{N}}^\dagger$ are given by

$$\begin{aligned} m_{\tilde{N}_0} &= |\mu| + m_Z^2 \frac{(I + \sin(2\beta))(\mu - M_1 \cos^2(\theta_W) - M_2 \sin^2(\theta_W))}{2(\mu - M_1)(\mu - M_2)} + ... \\ m_{\tilde{N}_1} &= |\mu| + m_Z^2 \frac{(I - \sin(2\beta))(\mu + M_1 \cos^2(\theta_W) + M_2 \sin^2(\theta_W))}{2(\mu + M_1)(\mu + M_2)} + ... \\ m_{\tilde{N}_2} &= M_1 - m_Z^2 \frac{\sin^2(\theta_W)(M_1 + \mu \sin(2\beta))}{\mu^2 - M_1^2} + ... \\ m_{\tilde{N}_3} &= M_2 - m_Z^2 \frac{\sin^2(\theta_W)(M_2 + \mu \sin(2\beta))}{\mu^2 - M_2^2} + ... \end{aligned} \tag{2.93}$$

where $\beta = \tan^{-1}(v_u/v_d)$, θ_W is the Weinberg angle and I is the sign of μ, assuming M_1 and M_2 to be positive and μ to be real. Here, the first two rows of (2.93) correspond to higgsino-like neutralinos while the third and fourth rows are bino- and wino-like respectively. The mass mixing terms (the fractions in 2.93) are assumed to be small in the limit that we are working in, so if $|\mu| \ll M_1, M_2$, the lightest neutralino will be the higgsino-like $\tilde{N}_0$.

Since it is usually assumed that DM is produced as a thermal relic, it is interesting to see what conditions need to be fulfilled for nearly pure higgsinos to have the correct relic density. In the limit of small neutralino mixing, we have [69]

$$\Omega_{\tilde{H}} h^2 = 0.1 \left(\frac{\mu}{1\text{ TeV}}\right)^2 \frac{1}{R_{\tilde{H}}}, \tag{2.94}$$

where $\Omega_{\tilde{H}} h^2 \approx 0.12$ is the observed DM relic density and $R_{\tilde{H}} \approx 1$ is a constant. Therefore, to obtain the correct DM relic abundance with thermally produced higgsinos as the only DM component, the higgsino mass needs to be $|\mu| \approx 1$ TeV.

The mass splitting between the two higgsino-like states in the small $|\mu|$ limit is given by [17]

$$\begin{aligned} m_\delta \equiv m_{\tilde{N}_1} - m_{\tilde{N}_0} &= m_Z^2 \frac{\sin^2(\theta_W)}{M_1} + m_Z^2 \frac{\cos^2(\theta_W)}{M_2} + ... \\ &\approx \left[185 \left(\frac{10^7\text{ GeV}}{M_1}\right) + 647 \left(\frac{10^7\text{ GeV}}{M_2}\right)\right] \text{keV}, \end{aligned} \tag{2.95}$$

where $\sin^2(\theta_W) \approx 0.222$ and $m_Z \approx 91.2$ GeV, and higher-order terms are neglected. Clearly, it is possible for the parameters M_1 and M_2 to have values much larger than $|\mu| \approx 1$ TeV such that the mass splitting is $O(100)$ keV, which is what I study in this thesis. These conditions can arise in, for example, split supersymmetric models [70].

Next, we want to study the interaction between higgsinos and quarks, since this is what gives rise to the DM-nucleus interactions of relevance to this thesis. After electroweak symmetry breaking, the higgsino-like neutralinos become Majorana fermions. The leading contribution to their quark-interaction is Z-boson exchange. Due to the Majorana nature of the neutralinos, this process cannot be elastic at tree-level, since Majorana fermions cannot have vector interactions. However, processes at loop-level will still give rise to subdominant elastic interactions, with a cross section of approximately $\sigma_e \approx 10^{-47}$ cm^2 [71]. This is enough to thermalize higgsinos captured by the Sun, as discussed in section 2.3.2.

An expression for the total inelastic spin-independent cross section between higgsinos and a nucleus of mass m_T from Z boson exchange is [72]

$$\sigma_i = \frac{G_F^2}{8\pi} \left(N - (1 - 4\sin^2(\theta_W) Z)^2\right) \frac{m_{\tilde{N}_0}^2 m_T^2}{(m_{\tilde{N}_0} + m_T)^2}, \tag{2.96}$$

where N and Z are the number of neutrons and protons in the nucleus respectively and G_F is the Fermi constant. We now want to compare this to the EFT discussed in 2.4 by computing the total cross section using the EFT Mathematica package from [66]. Using ^{130}Xe as a representative example, (2.96) yields $\sigma_i \approx 10^{-39}$ cm^2,

which in the EFT corresponds to $c_1^0 \approx 0.35\, m_V^{-2}$, where $m_V = 246.2$ GeV is the Higgs field vacuum expectation value. This can be used to apply the model-independent results provided by EFT computations to the specific case of nearly pure higgsino DM.

3

Inelastic Dark Matter Detection Prospects

This chapter contains the main results of this thesis. Here, I calculate the rate of dark matter (DM) capture in the Sun in the effective theory of inelastic DM, which has previously not been done, focusing on the illustrative case of 1 TeV DM with spin $\frac{1}{2}$. These calculations are used to set limits on the coupling constants of the theory based on the null results from the neutrino telescope IceCube. Finally, I compare these limits to direct detection limits that I derive from the null results of the direct detection experiments CRESST, PICO and XENON1T. I find that for large mass splittings, neutrino telescopes set the most stringent limits on the coupling constants of the effective theory of inelastic DM for most operators. This result highlights an as of yet unexploited complementarity between direct detection experiments and neutrino telescopes.

In the first section of this chapter, the solar capture rates for the effective theory operators are computed for 1 TeV DM with spin $\frac{1}{2}$ and mass splittings between -300 and 550 keV. In addition to this, the isotopes that contribute the most to the capture rate for the different operators and mass splittings are listed.

In the second section, exclusion limits on the effective field theory coupling constants for 1 TeV DM with spin $\frac{1}{2}$ and mass splittings between 0 and 550 keV from the direct detection experiments XENON1T, PICO-60 and, when possible, CRESST-II, along with the indirect detection experiment IceCube are presented. Since the form factor for tungsten is not implemented in the Mathematica package used to compute event rates [66], CRESST is included only for coherent operators, for which the Helm form factor can be used. It should be noted that while both the CRESST and PICO experiments have published more recent results than those used in this thesis, the older results give stronger limits for the inelastic, high DM mass parameter space examined in this thesis. The newer PICO detector consists of C_3F_8 instead of C_3FI, where the absence of the high-mass iodine decreases the sensitivity to highly inelastic DM [37]. The new CRESST detector, CRESST-III, has a lower energy threshold compared to CRESST-II but a much smaller exposure. For light DM, the more recent results are stronger, but for heavy DM they are much weaker [41]. For XENON1T and IceCube the most recent results are used, as they give the most stringent limits for the parameter space examined. In addition to this, I also compute hypothetical limits from a high-recoil analysis of XENON1T, where I assume that the span of analyzed recoil energies is expanded as in a high-recoil study of the XENON100 data [73]. This is to illustrate the currently realistic bounds of how well direct detectors can constrain inelastic DM.

The results show that for isoscalar operators, IceCube currently gives the most stringent limits for part of the parameter space examined for all operators except $\hat{O}_6$ and $\hat{O}_{13}$. For the isovector case, the same applies for all operators except $\hat{O}_6$, $\hat{O}_9$ and $\hat{O}_{10}$. As an example, consider the isoscalar spin-independent operator $\hat{O}_1$. In the complete absence of an elastic DM-nucleus interaction, IceCube gives the most stringent limits for mass splittings of $m_\delta \gtrsim 325$ keV. If a subdominant elastic process exists and has a total cross section in the range of 10^{-49} cm$^2 \lesssim \sigma_e \lesssim 10^{-46}$ cm^2, IceCube gives the most stringent limits for $m_\delta \gtrsim 130$ keV.

3.1 Solar capture rates

In this section, the total solar capture rates for 1 TeV DM with spin $\frac{1}{2}$ and mass splittings between -300 and 550 keV for the operators described in section 2.4 are illustrated. The capture rates are computed by evaluating

$$C = \frac{\rho_\chi}{m_\chi} \sum_i \int_{r_{L,i}}^{r_\odot} dr 4\pi r^2 n_i(r) \int_{u_{m,i}(r)}^{u_+^{C,i}(r)} du \frac{f(u)}{u} w\, \Theta(E_H^i - E_c) \int_{E_L^i(u,r)}^{E_H^i(u,r)} dE_R \frac{d\sigma(w^2, E_R)}{dE_R}. \tag{3.1}$$

a formula derived in section 2.3.1, with the sum extending over the 15 most abundant elements in the Sun. To calculate the differential cross sections, I altered the Mathematica package described in [66] to consistently compute cross sections and experimental rates for inelastic DM. The altered code is given in appendix A. I used one-body density matrix elements for solar nuclei as computed in [67]. The nuclear densities and escape velocity are extracted from DarkSUSY, and come from the Standard Solar Model [63, 64]. In each capture scenario, the non-zero coupling constant is set to a reference value of $c_i = 10^{-3}\ m_V^{-2}$, where $m_V = 246.2$ GeV is the Higgs field vacuum expectation value. For the DM velocity distribution, the Standard Halo Model with a galactic escape velocity of 544 km/s and a solar velocity of 220 km/s is used [53].

The total solar capture rates for 1 TeV DM with mass splittings between -300 and 550 keV for all isoscalar operators are shown in figure 3.1. The corresponding capture rates for all isovector operators are given in figure 3.2. The nuclei that contribute the most to the capture rate for 1 TeV DM at some benchmark mass splittings between -300 and 550 keV for all isoscalar operators are shown in table 3.1. The corresponding nuclei for the isovector operators are given in table 3.2.

As can be seen from figures 3.1 and 3.2, the operators naturally split into two categories with 7 operators each. The first category consists of the operators that can capture DM up to high mass splittings, over 500 keV. These are $\hat{O}_1$, $\hat{O}_3$, $\hat{O}_5$, $\hat{O}_8$, $\hat{O}_{11}$, $\hat{O}_{12}$ and $\hat{O}_{15}$. The common property of these operators is that they do not have a direct proportionality to the nuclear spin (although some of them depend on it, but only through triple products). The solar nuclei of relevant density with the highest masses are iron (^{56}Fe) and nickel (^{58}Ni), both of which have spin zero ground states. As the mass splitting increases, the minimum nucleus mass that makes scattering kinematically allowed also increases, so for solar capture at high

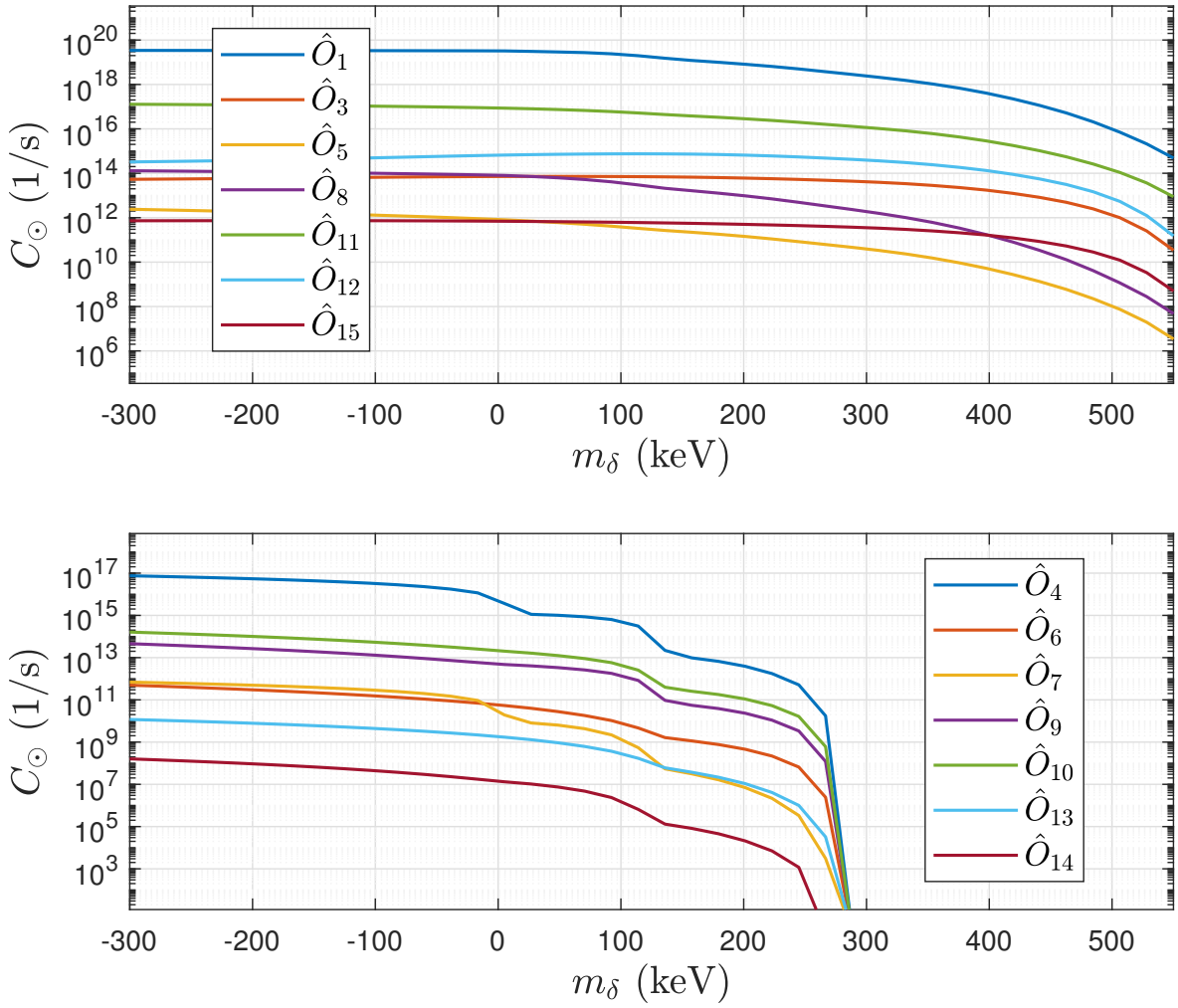

Figure 3.1: The total solar capture rate of 1 TeV DM for each isoscalar operator, assuming a coupling strength of $c_i = 10^{-3}$ (246.2 GeV)$^{-2}$.

mass splittings to be possible iron and nickel need to interact with DM. Therefore, the operators in this category are the ones that allow these heavy nuclei to interact with DM, and thus capture it.

The nuclei that contribute the most to the capture rate for some mass splitting and some interaction type for the operators in the first category are, in the isoscalar case, helium, nitrogen, oxygen, silicon and iron. The corresponding nuclei for the isovector case are hydrogen, aluminum, iron and nickel.

The second category includes the operators for which DM with high mass splittings is not captured. Specifically, for these operators the Sun is unable to capture DM with $m_\delta \gtrsim 285$ keV, which is the limit at which scattering with aluminum is kinematically forbidden. These are $\hat{O}_4$, $\hat{O}_6$, $\hat{O}_7$, $\hat{O}_9$, $\hat{O}_{10}$, $\hat{O}_{13}$ and $\hat{O}_{14}$. All of these operators have an overall nuclear spin-proportionality, and aluminum is the heaviest solar nucleus with non-zero spin of sufficient abundance to contribute to

$\hat{O}_i$ \ m_δ	-300	-213	-147	-60	5	92	158	245	310	397	463	550
$\hat{O}_1$	^{4}He	O	O	O	O	O	Fe	Fe	Fe	Fe	Fe	Fe
$\hat{O}_3$	Si	Si	Si	Fe	Fe	Fe	Fe	Fe	Fe	Fe	Fe	Fe
$\hat{O}_4$	H	H	H	H	H	N	Al	Al	–	–	–	–
$\hat{O}_5$	N	N	N	N	N	Fe	Fe	Fe	Fe	Fe	Fe	Fe
$\hat{O}_6$	N	N	N	N	N	N	Al	Al	–	–	–	–
$\hat{O}_7$	H	H	H	H	H	N	Al	Al	–	–	–	–
$\hat{O}_8$	N	N	N	N	N	Fe	Fe	Fe	Fe	Fe	Fe	Fe
$\hat{O}_9$	H	H	H	N	N	N	Al	Al	–	–	–	–
$\hat{O}_{10}$	N	N	N	N	N	N	Al	Al	–	–	–	–
$\hat{O}_{11}$	O	O	O	O	O	Fe	Fe	Fe	Fe	Fe	Fe	Fe
$\hat{O}_{12}$	Si	Si	Si	Fe	Fe	Fe	Fe	Fe	Fe	Fe	Fe	Fe
$\hat{O}_{13}$	N	N	N	N	N	N	Al	Al	–	–	–	–
$\hat{O}_{14}$	H	H	H	N	N	N	Al	Al	–	–	–	–
$\hat{O}_{15}$	Si	Fe	Fe	Fe	Fe	Fe	Fe	Fe	Fe	Fe	Fe	Fe

Table 3.1: The solar nucleus with the highest capture rate for all isoscalar operators for various values of the mass splitting m_δ, given in keV, for a DM mass of 1 TeV.

$\hat{O}_i$ \ m_δ	-300	-213	-147	-60	5	92	158	245	310	397	463	550
$\hat{O}_1$	H	H	H	H	H	Fe	Fe	Fe	Fe	Fe	Fe	Ni
$\hat{O}_3$	Fe	Fe	Fe	Fe	Fe	Fe	Fe	Fe	Fe	Fe	Fe	Fe
$\hat{O}_4$	H	H	H	H	H	Al	Al	Al	–	–	–	–
$\hat{O}_5$	Al	Al	Al	Al	Al	Al	Al	Al	Fe	Fe	Fe	Ni
$\hat{O}_6$	Al	Al	Al	Al	Al	Al	Al	Al	–	–	–	–
$\hat{O}_7$	H	H	H	H	H	Al	Al	Al	–	–	–	–
$\hat{O}_8$	Al	Al	Al	Al	Al	Al	Al	Al	Fe	Fe	Fe	Ni
$\hat{O}_9$	H	H	H	H	Al	Al	Al	Al	–	–	–	–
$\hat{O}_{10}$	H	H	H	H	Al	Al	Al	Al	–	–	–	–
$\hat{O}_{11}$	H	H	H	Fe	Fe	Fe	Fe	Fe	Fe	Fe	Fe	Ni
$\hat{O}_{12}$	Fe	Fe	Fe	Fe	Fe	Fe	Fe	Fe	Fe	Fe	Fe	Fe
$\hat{O}_{13}$	Al	Al	Al	Al	Al	Al	Al	Al	–	–	–	–
$\hat{O}_{14}$	H	H	H	H	Al	Al	Al	Al	–	–	–	–
$\hat{O}_{15}$	Fe	Fe	Fe	Fe	Fe	Fe	Fe	Fe	Fe	Fe	Fe	Fe

Table 3.2: The solar nucleus with the highest capture rate for all isovector operators for various values of the mass splitting m_δ, given in keV, for a DM mass of 1 TeV.

capture, which is why the capture rate goes to zero when scattering with aluminum is forbidden.

The nuclei that contribute the most to the capture rate for some mass split-

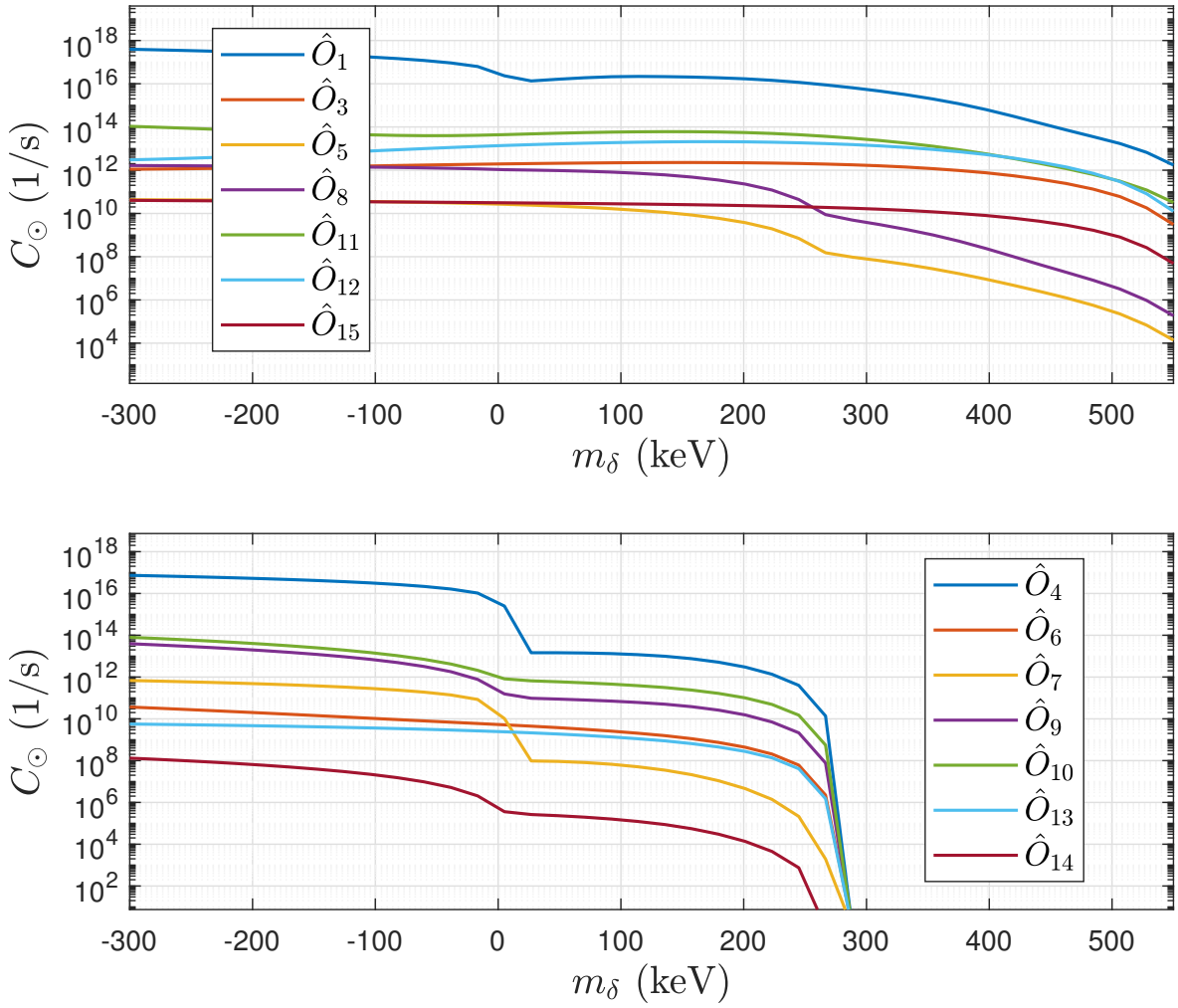

Figure 3.2: The total solar capture rate of 1 TeV DM for each isovector operator, assuming a coupling strength of $c_i = 10^{-3}$ (246.2 GeV)$^{-2}$.

ting and some interaction type for the operators in the second category are, in the isoscalar case, hydrogen, nitrogen and aluminum. The corresponding nuclei for the isovector case are hydrogen and aluminum.

Comparing figures 3.1 and 3.2, it is clear that the isoscalar operators are more efficient at capturing DM than their isovector counterparts. This is due to the fact that while isoscalar operators scale with the total number of nucleons in a nucleus, the isovector ones scale with the proton-neutron number difference. The total number of nucleons in the abundant solar nuclei are typically $O(10)$, with the maximum being 58 for nickel. The proton-neutron number difference, however, is zero for nine of the nuclei and at most 4, for iron and argon, making the isovector capture rate significantly lower.

3.2 Limits from detection experiments

In this section, I compute limits on the coupling constants in the effective field theory of inelastic DM-nucleon interaction for 1 TeV DM with spin $\frac{1}{2}$ and mass splittings between 0 and 550 keV, based on the null results from XENON1T [30, 31], PICO-60 [36], CRESST-II [40] and IceCube [49]. In addition to this, I perform a hypothetical high-recoil analysis of the XENON1T data based on the recoil energies used for a high-recoil study of XENON100 [73] to illustrate the possible improvement of XENON1T limits on inelastic DM. The analysis includes these experiments specifically as they combined provide the most stringent limits for the parameter space that I will examine.

For the direct detection experiments, I assume that the number of events follow a Poisson distribution, according to

$$P_M(N) = \frac{e^{-M} M^N}{N!}, \tag{3.2}$$

where N is the number of events, P_M the associated probability and M the mean of the distribution. If an experiment has observed N_e signal events, an interaction strength is considered excluded if it would yield M_e signal events, where

$$10\% = P_{M_e}(N \leq N_e) = \sum_{N=0}^{N_e} \frac{e^{-M_e} M_e^N}{N!}, \tag{3.3}$$

meaning that there is a 10% chance of having seen N_e events or fewer. Thus, this is a 90% confidence limit. For $N_e \geq 1$, (3.3) is a transcendental equation, but for our purposes it is enough to note that $N_e = 0$ gives $M_e = 2.3$ and $N_e = 4$ gives $M_e = 7.99$ [74], since XENON1T and PICO have both reported 0 signal events while CRESST has reported 4 signal events. This method gives limits that agree with the published XENON1T and PICO limits at zero mass splitting within a factor of 3. Since CRESST has not reported results for masses as high as those I study, there is nothing to compare to in this case.

The expected event rates for the direct detection experiments are computed with the Mathematica package described in [66], which I have extended for this thesis to consistently describe inelastic DM scattering. The most relevant parts of the code that I developed are included in appendix A. The energy ranges over which the differential rates are integrated for the different experiments are 5-40 keV for XENON1T [30], 10-1000 keV for PICO [36] and 0.3-120 keV for CRESST [40]. For the hypothetical high-recoil analysis of XENON1T, 5-240 keV is used [73]. For CRESST, the most relevant nucleus is tungsten (W), due to its high mass. However, the detailed nuclear form factor calculations that the Mathematica package provides are not implemented for W. Therefore, I instead use the Helm form factor when computing CRESST event rates. The Helm form factor is only valid for coherent interactions, i.e. those that simply scale as the number of nucleons squared. These are the operators which give rise to the DM particle response operator $R_M^{\tau\tau'}$. Specifically, they are $\hat{O}_1$, $\hat{O}_5$, $\hat{O}_8$ and $\hat{O}_{11}$.

For IceCube, capture rates are computed by the same method as in section 3.1 and the corresponding muon fluxes are computed using DarkSUSY [63, 64]. When

computing the exclusion limits, I consider both a best and worst case scenario, which give rise to the strongest and weakest limits possible respectively. For the best case scenario, the $\tau^-\tau^+$ annihilation channel is the one that I study as it gives the most stringent limits on the coupling constants, while I use the $b\bar{b}$ channel for the worst case, as it gives the weakest limits. Since the differences between the annihilation channels depend only on mass and not mass splitting, it is possible to convert between them by simply rescaling the limits I compute. To convert from $\tau^-\tau^+$ annihilation limits into corresponding ones for W^+W^- and $b\bar{b}$ annihilation, one multiplies with 1.8 and 11.18 respectively. Furthermore, due to the possibility that the DM annihilation in the Sun is not in equilibrium with the capture rate, the worst case scenario is based on a suppressed muon flux while the best case is based on an unsuppressed flux. The suppressed flux is computed using a suppression rate from Clementz and Blennow [62], with exponential extrapolation in the mass and mass splitting when needed as described in subsection 2.3.2. The suppression values that I use are based on the 10^{-45} cm^2 inelastic cross section results, and are therefore conservative, since a higher cross section would mean a lower suppression. The suppressed case corresponds to having no elastic interaction, while the unsuppressed case corresponds to having a subdominant elastic interaction with a very small cross section ($\sigma_e \gtrsim 10^{-49}$ cm^2). The exclusion limits are then computed using table 4 from [49]. This method yields limits that differ from the publish IceCube limits by at most 10% in the elastic case.

The exclusion limits on the isoscalar EFT coupling constants are presented in figures 3.3 and 3.4. The corresponding limits for the isovector case are given in figures 3.5 and 3.6. These figures are the main results of this thesis.

As a representative example, let us in detail examine the isoscalar $\hat{O}_1$. In the limit of elastic scattering, XENON1T gives the strongest direct detection limits. For mass splittings of $m_\delta \gtrsim 210$ keV, the maximum analyzed recoil energy E_R at XENON1T is too low for it to be an efficient probe, and PICO instead gives the strongest direct detection limit due to a very high maximum analyzed E_R. When $m_\delta \gtrsim 320$ keV, the high mass of tungsten means that CRESST gives the strongest direct detection limits. As a hypothetical, if XENON1T were to make a high-recoil analysis as was done for XENON100, it would give the most stringent limits for $m_\delta \lesssim 360$ keV before being overtaken by CRESST. It should be noted that, for recoil energy-independent operators like $\hat{O}_1$, the benefits of a high-recoil analysis do not become significant until $m_\delta \gtrsim 115$ keV. For parts of the parameter space the indirect detection experiment IceCube sets the strongest limits on the DM-nucleon interaction, even if XENON1T makes a high-recoil analysis. For the worst case scenario, IceCube gives the most stringent limits for mass splittings of $m_\delta \gtrsim 360$ keV. For the best case scenario, IceCube gives the most stringent limits for $m_\delta \gtrsim 150$ keV. As an example of a specific model constrained by this result, consider nearly pure higgsino DM. As discussed in section 2.5, such DM is expected to have a big enough elastic cross section for solar annihilation and capture to be in equilibrium, leading to an unsuppressed muon flux, mainly annihilates into W^+W^- and should have a coupling constant of $c_1^0 \approx 0.35\ m_V^{-2}$. Therefore, it is excluded for mass splittings up to 530 keV by IceCube, whereas previous analyses which only examined direct detection results could only exclude it up to 220 keV [17], and a high-recoil analysis

of XENON1T would exclude it up to 320 keV.

When describing the results, the different effective theory interactions can be grouped into two categories (as in the previous subsection) based on the operators themselves, and further divided into subgroups based on the exclusion plots in figures 3.3-3.6. The first category consists of the operators that do not have an overall nuclear spin-dependence. For all these operators, as for $\hat{O}_1$ which was discussed above, direct detection experiments are superior in the elastic limit, but the indirect detection experiment IceCube sets the strongest limits for high mass splittings. The operators in this category are $\hat{O}_1$, $\hat{O}_3$, $\hat{O}_5$, $\hat{O}_8$, $\hat{O}_{11}$, $\hat{O}_{12}$ and $\hat{O}_{15}$. Looking at the explicit forms given in 2.1, none of them depend on the nuclear spin except through triple products, meaning that they do not have an overall proportionality to the spin. This means that ^{56}Fe and ^{58}Ni, both of which have spin zero nuclear ground states, are activated by these operators. Since iron and nickel are the heaviest elements of relevant density in the Sun, this is a necessary condition for the Sun to be able to capture inelastic DM with large mass splittings.

The second category consists of the operators that do scale with the nuclear spin, and therefore activate neither iron nor nickel which both have spin zero nuclear ground states. For these operators, IceCube becomes insensitive to inelastic DM with $m_\delta \gtrsim 285$ keV, which is the mass splitting where aluminum, the heaviest solar nucleus with a non-trivial spin, is no longer able to capture DM. The operators in this category are $\hat{O}_4$, $\hat{O}_6$, $\hat{O}_7$, $\hat{O}_9$, $\hat{O}_{10}$, $\hat{O}_{13}$ and $\hat{O}_{14}$. The nuclear spin-proportionality of these operators means that hydrogen is a relevant nucleus for DM capture in the elastic and exothermic ($m_\delta < 0$) cases. But, even for small positive mass splittings, as low as $m_\delta \gtrsim 10$ keV, hydrogen becomes ineffective, and nitrogen and aluminum are instead the nuclei contributing the most to the capture rate. Based on the exclusion limits, the operators in this category can be further divided into two subgroups. The first subgroup is the operators where IceCube sets the strongest limits on elastic 1 TeV DM, even if XENON1T were to make a high-recoil analysis. For the isoscalar case, these are $\hat{O}_4$, $\hat{O}_7$ and $\hat{O}_{14}$. For the isovector case, IceCube sets the strongest limits only for $\hat{O}_7$. The operators $\hat{O}_4$ and $\hat{O}_7$ are not only nuclear spin-dependent, but they are also independent of the momentum transfer.

The remaining nuclear spin-dependent operators fall in the second subgroup, consisting of operators where IceCube does not give the most stringent limits for elastic DM. For the isoscalar case, $\hat{O}_6$, $\hat{O}_9$, $\hat{O}_{10}$ and $\hat{O}_{13}$ fall into this category. However, for both $\hat{O}_9$ and $\hat{O}_{10}$ IceCube gives the strongest limits in the best case scenario for a small positive mass splitting, but would not do so if a high-recoil analysis of XENON1T were made. For the isovector case $\hat{O}_4$, $\hat{O}_6$, $\hat{O}_9$, $\hat{O}_{10}$ and $\hat{O}_{13}$ and $\hat{O}_{14}$ are in this category. Without a high-recoil XENON1T analysis, IceCube gives the strongest limits for the elastic case for $\hat{O}_4$. All of the isovector operators in this subgroup, except for $\hat{O}_4$, are momentum transfer-dependent. For all of these except for $\hat{O}_6$, there is actually an intermediate mass splitting range where IceCube is particularly competitive, around 100-250 keV.

As is clear from the discussion above, neutrino telescope limits for isovector couplings are less competitive than for their isoscalar counterparts. The reason for this is that the proton-neutron difference among solar nuclei is comparatively low. For many of the most abundant solar nuclei, the difference is 0, and the maximum dif-

ference is 4 (for iron and argon). In contrast, all xenon isotopes have a difference of at least 16, while tungsten has at least 32. Since isovector interactions scale with this difference, the direct detectors are more sensitive to them.

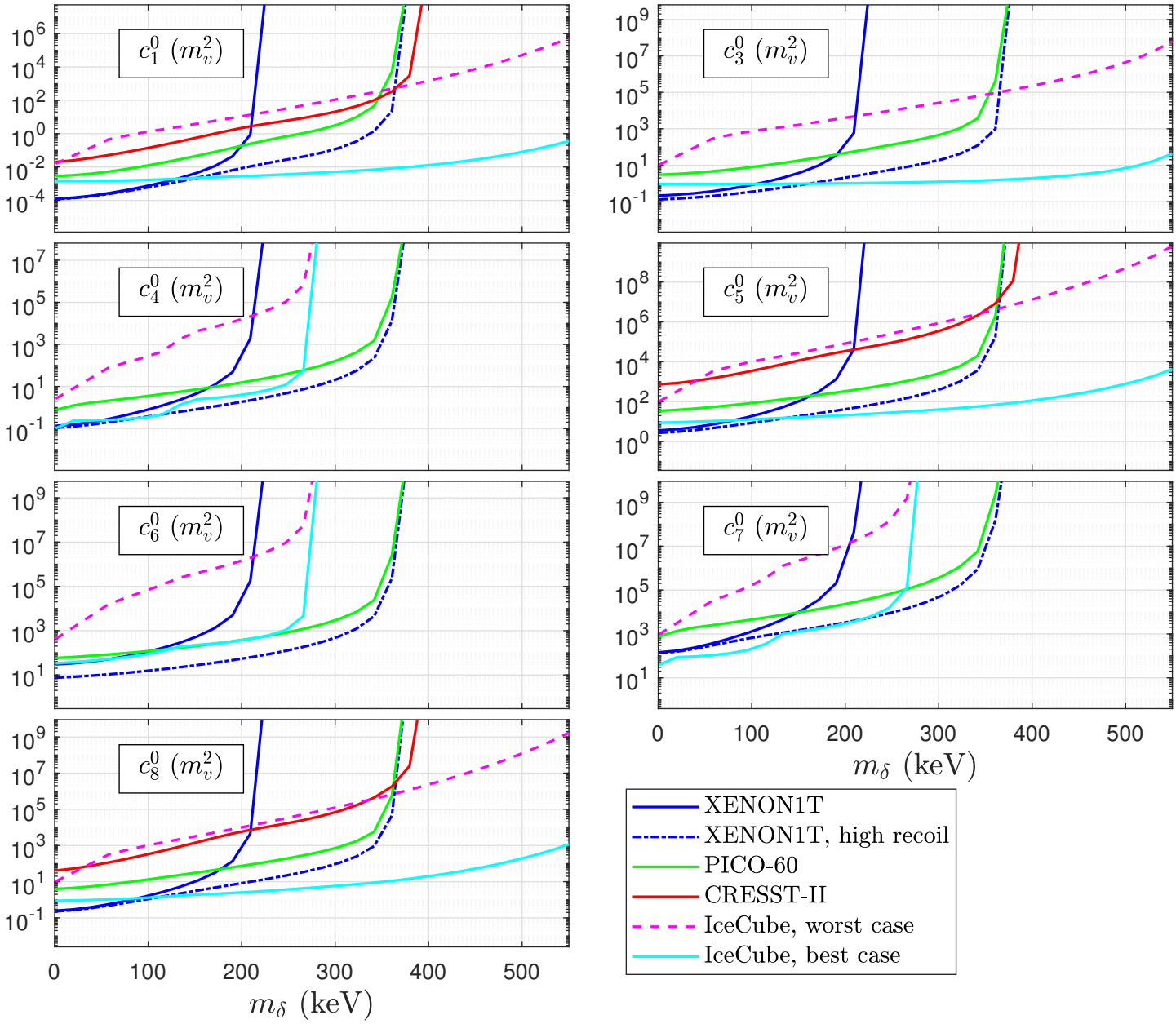

Figure 3.3: Constraints on the isoscalar effective theory coupling constants for operators $\hat{O}_1$ to $\hat{O}_8$ for 1 TeV DM at a 90% confidence level from XENON1T, a hypothetical high-recoil analysis of XENON1T, PICO-60, CRESST-II and IceCube.

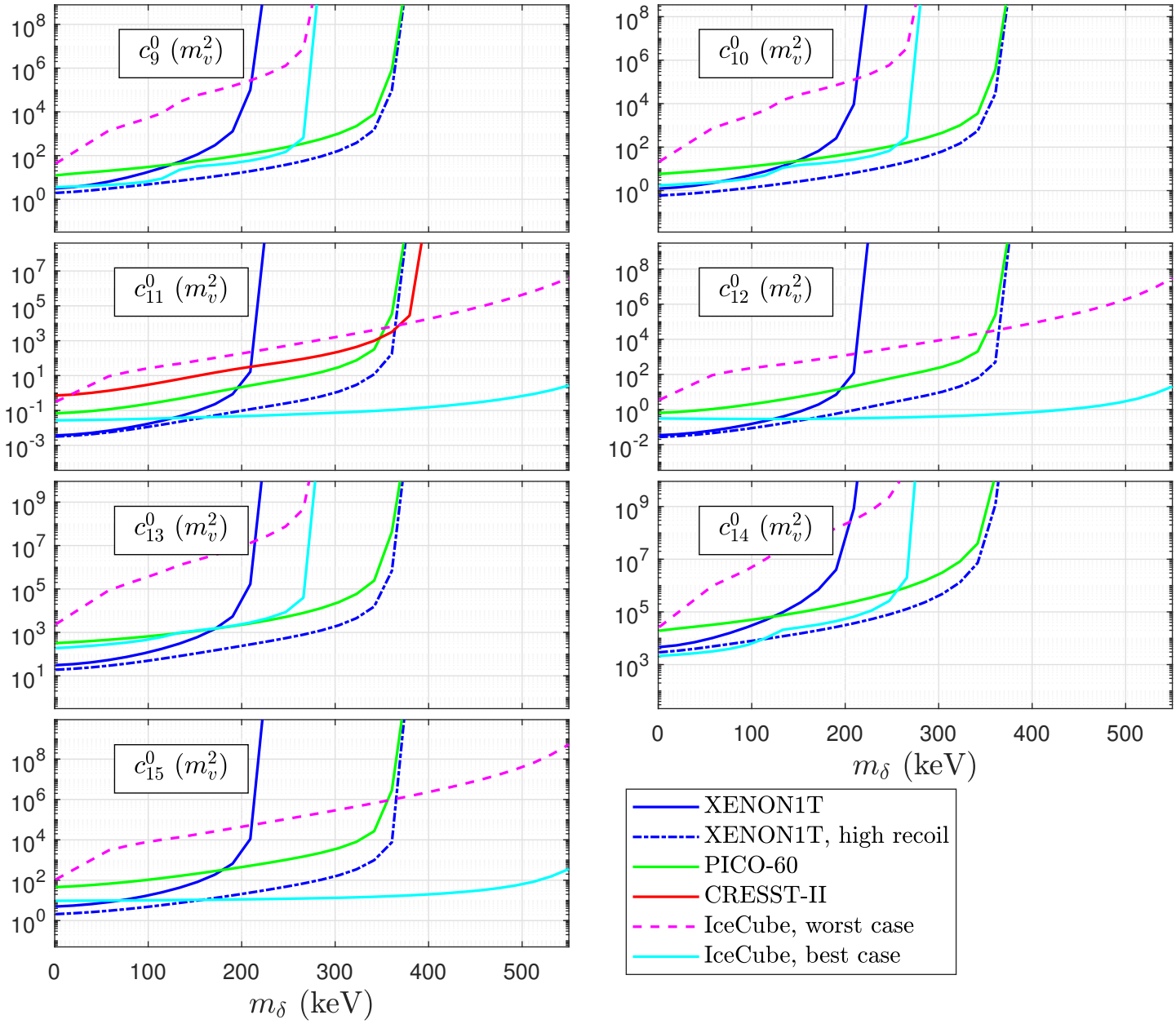

Figure 3.4: Constraints on the isoscalar effective theory coupling constants for operators $\hat{O}_9$ to $\hat{O}_{15}$ for 1 TeV DM at a 90% confidence level from XENON1T, a hypothetical high-recoil analysis of XENON1T, PICO-60, CRESST-II and IceCube.

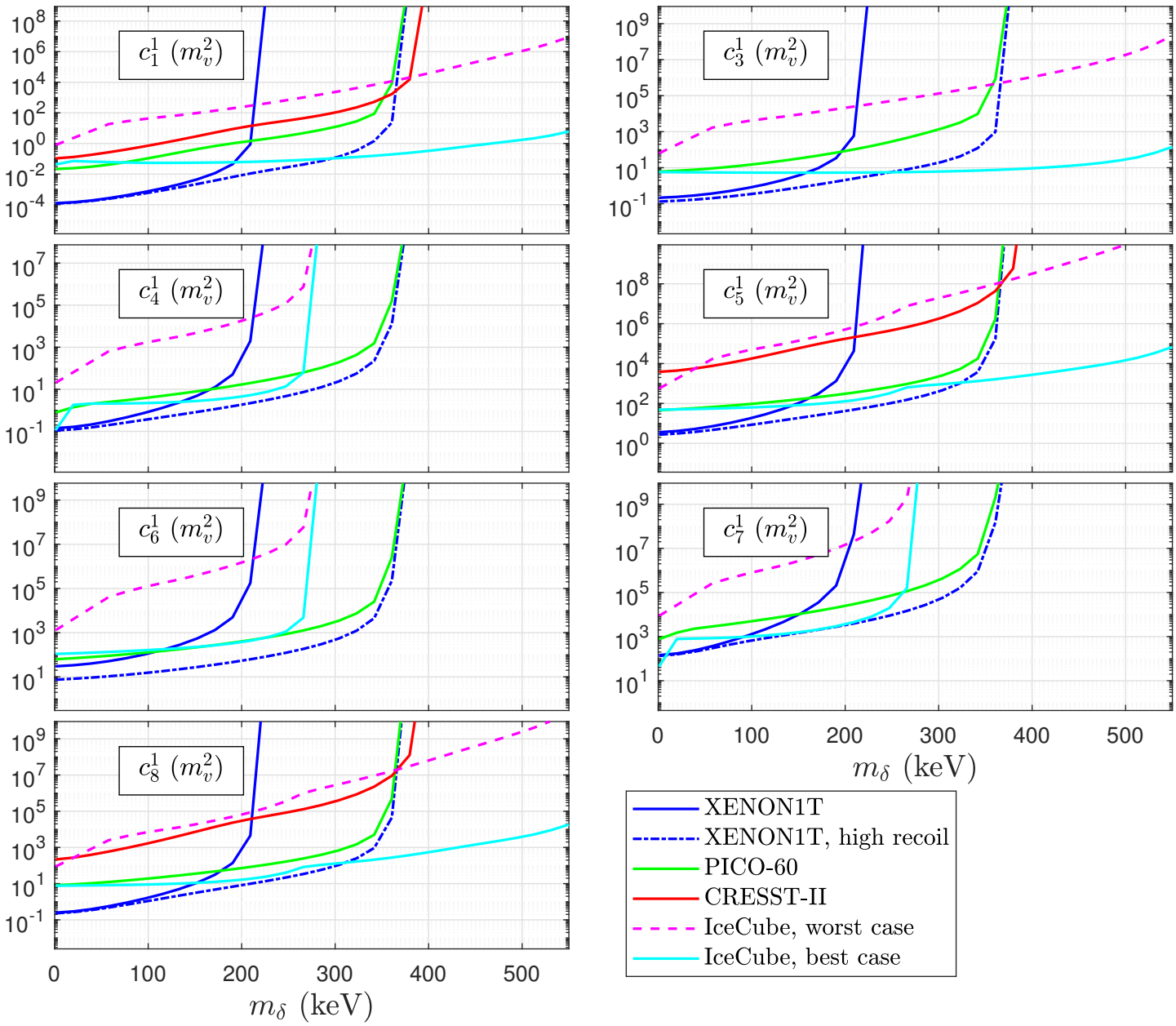

Figure 3.5: Constraints on the isovector effective theory coupling constants for operators $\hat{O}_1$ to $\hat{O}_8$ for 1 TeV DM at a 90% confidence level from XENON1T, a hypothetical high-recoil analysis of XENON1T, PICO-60, CRESST-II and IceCube.

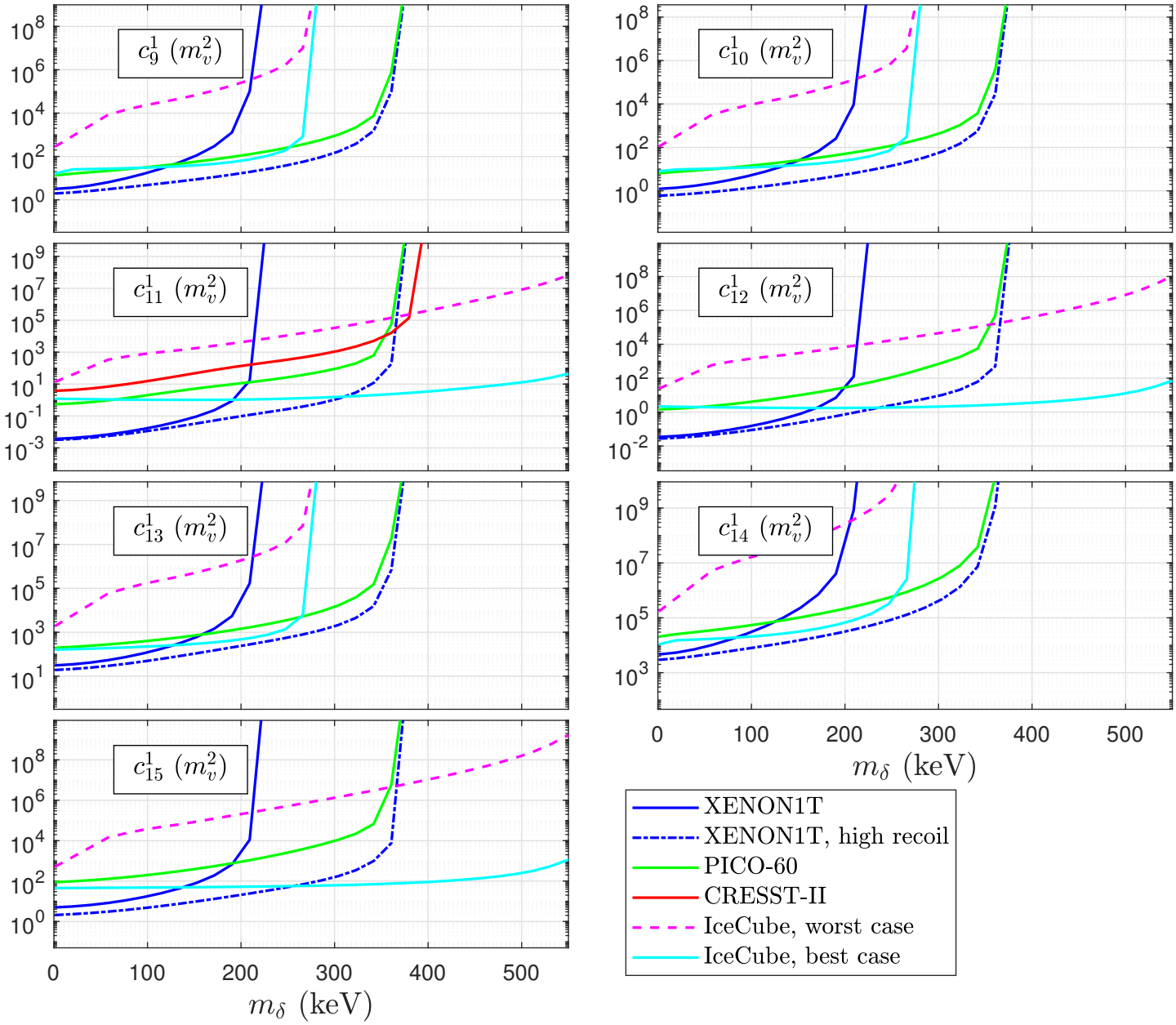

Figure 3.6: Constraints on the isovector effective theory coupling constants for operators $\hat{O}_9$ to $\hat{O}_{15}$ for 1 TeV DM at a 90% confidence level from XENON1T, a hypothetical high-recoil analysis of XENON1T, PICO-60, CRESST-II and IceCube.

4

Discussion and Conclusion

In this thesis, I have studied inelastic dark matter (DM). In particular, I have computed the solar capture rate for all possible DM-nucleon interactions mediated by a heavy particle of at most spin 1 as a function of the DM mass, the mass splitting between the initial and final DM states and the DM-nucleon cross section. Based on these calculations, I have computed exclusion limits on the effective field theory coupling constants for spin $\frac{1}{2}$ DM with a mass of 1 TeV and mass splittings between 0 and 550 keV derived from the null result from IceCube. This limit of high DM mass and mass splittings is sometimes referred to as the *inelastic frontier* [17]. As a comparison, I have also computed corresponding exclusion limits from the most competitive direct detection experiments for these parameters, specifically CRESST, PICO and XENON1T. I computed the IceCube limits both for a best case where the solar DM annihilation is unsuppressed with a hard annihilation channel ($\tau^+\tau^-$) and a worst case where it is suppressed as a function of the DM mass and mass splitting with a weak annihilation channel ($b\bar{b}$). The unsuppressed case arises when a sufficiently strong elastic interaction allows DM to thermalize in the sun, whereas the suppressed case lacks such an interaction, leading to weaker annihilation signals than in the unsuppressed case. The results thus obtained show that IceCube gives the most stringent limits on the coupling constants for parts of the inelastic DM parameter space for the majority of the effective field theory operators, especially the isoscalar ones. As an example of a specific model which is constrained by these results, nearly pure higgsino DM is excluded for mass splittings up to 530 keV, whereas previous analyses excluded it only up to 220 keV [17]. These results are novel, and provide the insight that neutrino telescopes are highly significant when inelastic DM models are considered. Furthermore, the solar inelastic DM capture rate has in the literature previously been presented only for the standard spin-independent and spin-dependent interactions [54, 60, 61], whereas in this thesis, I present it for a much wider range of DM-nucleus interactions.

It should be noted that it is not entirely proper to consider single effective field theory operators at a time, as in this thesis, since they in general will tend to have some dependence on each other when interpreted as low-velocity limits of a full, high-energy theory [75]. However, if one considers a set of many operators with a given proportionality between the coupling constants, it is possible to use the results computed in chapter 3 to draw conclusions for this set by parameterizing the coupling constants.

One significant issue regarding the interpretation of IceCube data and its relation to inelastic DM is the issue of solar thermalization of inelastic DM. In most analyses of the solar annihilation of inelastic DM, it is assumed that the DM is thermalized,

as in the elastic case, motivated by more-or-less hand-wavy arguments. However, recent results by Clementz and Blennow [62] indicate that inelastic DM only thermalizes when the mass splitting is very small or if there is a subdominant elastic cross section of sufficient size. They find that, in the absence of such an interaction, the annihilation signal is severely suppressed for much of the parameter space. In this thesis, I have computed specific values for this suppression by extrapolating the results given in [62], which naturally introduces a big uncertainty. Furthermore, I have computed the suppression assuming an inelastic DM-nucleon cross section of $\sigma_i = 10^{-45}$ cm^2, which simplifies the analysis compared to adjusting the suppression based on the derived limits. Higher cross sections would yield a lower suppression, meaning that this simplification gives a conservative estimate for the derived limits (assuming that the total inelastic cross section $\sigma_i > 10^{-45}$ cm^2). For a more proper analysis, the suppression needs to be computed for a wider range of parameters and greater care needs to be taken with regards to the dependence of the signal suppression on the elastic and inelastic cross sections, and both of these have to specified when constraining models. It should however be noted that inelastic DM models that have a subdominant elastic cross section which is greater than $\sim 10^{-50}\,(m_\chi/\text{GeV})$ cm^2 do not suffer from these complications, as this elastic cross section is enough for thermalization to occur, even in the complete absence of an inelastic interaction [61]. If a more exact value of this lower limit and its dependence on the inelastic cross section is determined by future research, this would further clarify more precisely which inelastic DM models are constrained by neutrino telescope experiments and which are not.

As discussed in [17], direct detection experiments tend to not analyze their data up to particularly high recoil energies. Since DM-nucleus scattering at the inelastic frontier has a higher recoil energy threshold than for the elastic case, direct detectors become insensitive to these types of models if the mass splitting exceeds a couple of hundred keV, in part due to the small span of recoil energies analyzed. Since then, high-recoil studies have been made [73, 76]. However, as shown in this thesis, direct detectors are inferior to neutrino telescopes for most interaction types even when high recoil energies are analyzed. To illustrate this I computed hypothetical XENON1T limits assuming a maximum recoil energy of 240 keV, as was used in the XENON100 high-recoil analysis [73], and 0 observed events. This hypothetical result gave the strongest limits for part of the parameter space for a few interaction types, but it is completely insensitive to DM with $m_\delta \gtrsim 380$ keV. Furthermore, it could only exclude nearly pure higgsino models up to 320 keV, whereas IceCube already excludes it up to 530 keV.

The reason for this neutrino telescope advantage is the gravitational potential of the Sun. Since there is a minimum DM speed for scattering to be possible, which increases with the mass splitting, terrestrial detectors become entirely blind to inelastic DM models where this minimum speed is greater than the local speed of all DM particles. This is less limiting when it comes to solar scattering, since the speed of DM that reaches the Sun is greatly increased due to its high gravitational pull. Therefore, the mass splitting at which solar inelastic scattering is impossible is much higher than the corresponding one for terrestrial detector scattering. Despite the signal suppression discussed above, this makes neutrino telescope experiments

indispensable when studying DM models at the inelastic frontier.

Bibliography

[1] G. Bertone and D. Hooper. History of dark matter. `arXiv:1605.04909`, 2016.

[2] F. Zwicky. Die rotverschiebung von extragalaktischen nebeln. *Helvetica Physica Acta*, 6, 110, 1933.

[3] D. Clowe, A. Gonzalez, and M. Markevitch. Die rotverschiebung von extragalaktischen nebeln. *Astrophys J.*, 604, 2004.

[4] X ray: NASA/CXC/CfA/M.Markevitch et al.; Optical: NASA/STScI; Magellan/U.Arizona/D.Clowe et al.; Lensing Map: NASA/STScI; ESO WFI; Magellan/U.Arizona/D.Clowe et al. Bullet cluster. *Wikimedia Commons*, 2006.

[5] V. Rubin and W. Ford. Rotation of the andromeda nebula from a spectroscopic survey of emission regions. *Astrophys J.*, 159, 1970.

[6] M. Milgrom. A modification of the newtonian dynamics as a possible alternative to the hidden mass hypothesis. *Astrophys J.*, 270, 1983.

[7] J.D. Bekenstein. Rotation of the andromeda nebula from a spectroscopic survey of emission regions. *Phys. Rev. D*, 70, 2004.

[8] P. van Dokkum et al. A galaxy lacking dark matter. *Nature*, 555:629–632, 2018.

[9] B. Famaey, S. McGaugh, and M. Milgrom. MOND and the dynamics of ngc1052-df2. `arXiv:1804.04167`, 2018.

[10] J.R. Primack. Dark matter and structure formation in the universe. `arXiv:astro-ph/9707285`, 1997.

[11] A.A. Penzias and R.W. Wilson. A measurement of excess antenna temperature at 4080 mc/s. *Astrophys J.*, 142, 1965.

[12] A.A. Penzias and R.W. Wilson. Planck 2015 results. xiii. cosmological parameters. *Astronomy and Astrophysics*, 13, 2016.

[13] H. Okada, Y. Orikasa, and T. Toma. Nonthermal dark matter models and signals. *Phys. Rev. D*, 93, 2016.

[14] R.T. D'Agnolo, D. Pappadopulo, and J.T. Ruderman. Fourth exception in the calculation of relic abundances. *Phys. Rev. Lett.*, 119, 2017.

[15] G. Bertone, D. Hooper, and J. Silk. Particle dark matter: evidence, candidates and constraints. *Physics Reports*, 405(5), 2005.

[16] Y. Cui, D.E. Morrissey, D. Poland, and L. Randall. Candidates for inelastic dark matter. *Journal of High Energy Physics*, 2009(05), 2009.

[17] J. Bramante, P.J. Fox, G.D. Kribs, and A. Martin. The inelastic frontier: Discovering dark matter at high recoil energy. *Phys. Rev. D*, 64, 2011.

[18] K.N. Abazajian. Sterile neutrinos in cosmology. *Physics Reports*, 711-712, 2017.

[19] S. Dodelson and L.M. Widrow. Sterile neutrinos as dark matter. *Phys. Rev. Lett.*, 72, 1994.

[20] S.P. Martin. *A Supersymmetry Primer*. World Scientific, 2011.

[21] G. Jungman, M. Kamionkowski, and K. Griest. Supersymmetric dark matter. *Physics Reports*, 267(5), 1996.

[22] J.L. Hall and Y. Nomura. Spread supersymmetry. *Journal of High Energy Physics*, 2012, 1, 2012.

[23] D. Smith and N. Weiner. Inelastic dark matter. *Phys. Rev. D*, 64, 2001.

[24] L.J. Rosenberg and K.A. van Bibber. Searches for invisible axions. *Phys Rept.*, 325, 2000.

[25] E.W. Kolb and R. Slansky. Dimensional reduction in the early universe: Where have the massive particles gone? *Physics Letters B*, 135(5), 1984.

[26] S. Chang, N. Weiner, and I. Yavin. Magnetic inelastic dark matter. *Phys. Rev. D*, 82, 2010.

[27] T.M. Undagoitia and L. Rauch. Dark matter direct-detection experiments. `arXiv:1509.08767v2`, 2017.

[28] L. Baudis. Direct dark matter detection: The next decade. *Physics of the Dark Universe*, 1, 2012.

[29] A. Bolozdynya. Two-phase emission detectors and their applications. *Nucl. Instrum. Meth. Phys. Res. A*, 422, 1999.

[30] The XENON Collaboration: E. Aprile et al. First dark matter search results from the xenon1t experiment. *Phys. Rev. Lett.*, 119, 181301, 2017.

[31] The XENON Collaboration: R. Lang et al. Xenon1t probes deeper into dark matter wimps, with 1300 kg of cold xe atoms. `https://science.purdue.edu/xenon1t/?p=1080`. Accessed: 2018-05-31.

[32] PandaX Collaboration: X. Cao et al. PandaX: a liquid xenon dark matter experiment at CJPL. *Science China Physics, Mechanics & Astronomy*, 57(8), 2014.

[33] LUX Collaboration: D.S. Akerib et al. First results from the LUX dark matter experiment at the sanford underground research facility. *Phys. Rev. Lett.*, 112, 2014.

[34] PICO collaboration. Pico experiment. `http://www.picoexperiment.com`. Accessed: 2018-04-25.

[35] COUPP Collaboration: E. Behnke et al. First dark matter search results from a 4-kg cf3i bubble chamber operated in a deep underground site. *Phys. Rev. D*, 86, 2012.

[36] PICO Collaboration: C. Amole et al. Dark matter search results from the pico-60 cf3i bubble chamber. *Phys. Rev. D*, 93, 2016.

[37] PICO Collaboration: C. Amole et al. Dark matter search results from the pico-60 c3f8 bubble chamber. *Phys. Rev. Lett.*, 118, 2017.

[38] CRESST collaboration. Cresst - cryogenic rare event search with superconducting thermometers. `https://www.cresst.de`. Accessed: 2018-04-25.

[39] The CDMS II Collaboration: J. Cooley et al. Dark matter search results from the CDMS II experiment. *Science*, 327(5973), 2010.

[40] CRESST Collaboration: G. Angloher et al. Results on light dark matter particles with a low-threshold cresst-ii detector. *Eur. Phys. J. C*, 76:25, 2016.

[41] CRESST Collaboration: F. Petricca et al. First results on low-mass dark matter from the cresst-iii experiment. `arXiv:1711.07692`, 2016.

[42] J.M. Gaskins. A review of indirect searches for particle dark matter. *Contemporary Physics*, 57(4), 2016.

[43] S. Palomares-Ruiz and J.M. Siegal-Gaskins. Annihilation vs. decay: constraining dark matter properties from a gamma-ray detection. *JCAP*, 2010(07), 2010.

[44] Fermi-LAT collaboration: M. Ackermann et al. The fermi large area telescope on orbit: Event classification, instrument response functions, and calibration. *The Astrophysical Journal Supplement Series*, 203(1), 2012.

[45] PAMELA Collaboration: P. Picozza et al. PAMELA – a payload for antimatter matter exploration and light-nuclei astrophysics. *Astroparticle Physics*, 27(4), 2007.

[46] A. Kounine. The alpha magnetic spectrometer on the international space station. *International Journal of Modern Physics E*, 21(08), 2012.

[47] R. Catena. Dark matter signals at neutrino telescopes in effective theories. *JCAP*, 1504, 2015.

[48] The Super-K Collaboration: S. Fukuda et al. The super-kamiokande detector. *Nucl. Instr. Meth. in Phys. Res. A*, 501, 2003.

[49] IceCube Collaboration: M.G. Aartsen et al. Search for annihilating dark matter in the sun with 3 years of icecube data. *Eur. Phys. J. C*, 77:146, 2017.

[50] V.A. Mitsou. Overview of searches for dark matter at the LHC. *Journal of Physics: Conference Series*, 651(1), 2014.

[51] S.-H. Kang, S. Scopel, and J.-H. Yoon. Explaining DAMA with proton-philic spin-dependent inelastic dark matter (pSIDM): a frequentist analysis. `arXiv:1801.02905`, 2018.

[52] G. Barello, S. Chang, and C.A. Newby. A model independent approach to inelastic dark matter scattering. *Phys. Rev. D*, 90, 2014.

[53] A.M Green. Astrophysical uncertainties on the local dark matter distribution and direct detection experiments. *Journal of Physics G*, 44(8), 2017.

[54] M. Blennow, S. Clementz, and J. Herrero-Garcia. Pinning down inelastic dark matter in the sun and in direct detection. *JCAP*, 2016(04), 2016.

[55] J.D. Lewin and P.F. Smith. Review of mathematics, numerical factors, and corrections for dark matter experiments based on elastic nuclear recoil. *Astroparticle Physics*, 6, 1996.

[56] A. Gould. Resonant enhancements in weakly interacting massive particle capture by the earth. *The Astrophysical Journal*, 321, 1987.

[57] NASA. Sun fact sheet. `https://nssdc.gsfc.nasa.gov/planetary/factsheet/sunfact.html`. Accessed: 2018-04-25.

[58] A. Gould and G. Raffelt. Thermal conduction by massive particles. *The Astrophysical Journal*, 352, 1990.

[59] A. Widmark. Thermalization time scales for wimp capture by the sun in effective theories. *JCAP*, 2017, 2017.

[60] S. Nussinov, L. Wang, and I. Yavin. Capture of inelastic dark matter in the sun. *JCAP*, 0908, 037, 2009.

[61] A. Menon, R. Morris, A. Pierce, and N. Weiner. Capture and indirect detection of inelastic dark matter. *Phys. Rev. D*, 82, 015011, 2010.

[62] M. Blennow, S. Clementz, and J. Herrero-Garcia. The distribution of inelastic dark matter in the sun. `arXiv:1802.06880`, 2018.

[63] P. Gondolo, J. Edsjö, P. Ullio, L. Bergström, M. Schelke, and E.A. Baltz. DarkSUSY: computing supersymmetric dark matter properties numerically. *JCAP*, 2004(07), 2004.

[64] J. Edsjö, T. Bringmann, P. Gondolo, P. Ullio, L. Bergström, M. Schelke, E.A. Baltz, and G. Duda. DarkSUSY homepage. `http://www.darksusy.org/`. Accessed: 2018-04-25.

[65] A.L. Fitzpatrick, W. Haxton, E. Katz, N. Lubbers, and Y. Xu. The effective field theory of dark matter direct detection. *JCAP*, 1302, 2013.

[66] N. Anand, A.L. Fitzpatrick, and W.C. Haxton. Model-independent wimp scattering responses and event rates: A mathematica package for experimental analysis. *Phys. Rev. D*, 89, 2014.

[67] R. Catena and B. Schwabe. Form factors for dark matter capture by the sun in effective theories. *JCAP*, 1504, 2015.

[68] J. Terning. *Modern Supersymmetry: Dynamics and Duality.* Oxford Science Publications, 2005.

[69] N. Arkani-Hamed, A. Delgado, and G.F. Giudice. The well-tempered neutralino. *Nuclear Physics B*, 741, 2006.

[70] P.J. Fox, G.D. Kribs, and A. Martin. Split dirac supersymmetry: An ultraviolet completion of higgsino dark matter. *Phys. Rev. D*, 90, 2014.

[71] J. Hisano, K. Ishiwata, N. Nagata, and T. Takesako. Direct detection of electroweak-interacting dark matter. *Journal of High Energy Physics*, (7), 2011.

[72] N. Nagata and S. Shirai. Higgsino dark matter in high-scale supersymmetry. *Journal of High Energy Physics*, (1), 2015.

[73] The XENON Collaboration: E. Aprile et al. Effective field theory search for high-energy nuclear recoils using the xenon100 dark matter detector. *Phys. Rev. D*, 96, 042004, 2017.

[74] J.W. Rohlf. Modern physics from a to z0. *Wiley*, 1994.

[75] F. Bishara, J. Brod, B. Grinstein, and J. Zupan. From quarks to nucleons in dark matter direct detection. *Journal of High Energy Physics*, (11), 2017.

[76] PandaX-II Collaboration: Xun Chen et al. Exploring the dark matter inelastic frontier with 79.6 days of pandax-ii data. *Phys. Rev. D*, 96, 102007, 2017.

A

Appendix: Mathematica codes

In this appendix, some of the numerical tools developed for this thesis are presented. First, the most relevant new functions based on the Mathematica package described in [66], extended by me to consistently describe inelastic DM scattering, are shown. The functions are used to compute form factors and the differential cross section respectively. After that, I give the Mathematica notebook that was used to compute the capture rates in section 3.1.

```
(*Function for computing inelastic form factors*)
FFfinalInel[DMmtx_,J_,T_]:=Block[{ii,jj,ResCoeff,
iiResponse,vmsq},

cvec[1]=cpvector;
cvec[2]=cnvector;
vmsq = (mdelta/q + q/(2MuT[mX,M]))^2;

ResCoeff[MJ]=Table[1/4 Cl[jchi]((cvec[ii][[5]]
cvec[jj][[5]] q^2+cvec[ii][[8]]cvec[jj][[8]])
(v^2-vmsq)+cvec[ii][[11]]cvec[jj][[11]]q^2)+
(cvec[ii][[2]](v^2-vmsq)+cvec[ii][[1]])
(cvec[jj][[2]](v^2-vmsq)+cvec[jj][[1]]),{ii,2},{jj,2}];

ResCoeff[SigmaPPJ]=Table[1/16 Cl[jchi](cvec[ii][[6]]
cvec[jj][[6]]q^4+(cvec[ii][[13]]cvec[jj][[13]]q^2+
cvec[ii][[12]]cvec[jj][[12]])(v^2-vmsq)+
2cvec[ii][[4]]cvec[jj][[6]]q^2+cvec[ii][[4]]cvec[jj][[4]])+
1/4 cvec[ii][[10]]cvec[jj][[10]]q^2,{ii,2},{jj,2}];

ResCoeff[SigmaPJ]=Table[1/32 Cl[jchi](2cvec[ii][[9]]
cvec[jj][[9]]q^2+(cvec[ii][[15]]cvec[jj][[15]]q^4+
cvec[ii][[14]]cvec[jj][[14]]q^2-2cvec[ii][[12]]
cvec[jj][[15]]q^2+cvec[ii][[12]]cvec[jj][[12]])(v^2-vmsq)+
2cvec[ii][[4]]cvec[jj][[4]])+1/8 (cvec[ii][[3]]cvec[jj][[3]]
q^2+cvec[ii][[7]]cvec[jj][[7]])(v^2-vmsq),{ii,2},{jj,2}];

ResCoeff[DeltaJ]=Table[q^2/(4mN^2) Cl[jchi](cvec[ii][[5]]
cvec[jj][[5]]q^2+cvec[ii][[8]]cvec[jj][[8]])+2 q^2/mN^2
cvec[ii][[2]]cvec[jj][[2]](v^2-vmsq),{ii,2},{jj,2}];
```

```
ResCoeff[PhiPPJ]=Table[q^2/(16mN^2) Cl[jchi](cvec[ii][[12]] -
cvec[ii][[15]]q^2)(cvec[jj][[12]] - cvec[jj][[15]]q^2)+
q^4/(4mN^2)cvec[ii][[3]]cvec[jj][[3]],{ii,2},{jj,2}];

ResCoeff[PhiTPJ]=Table[q^2/(16mN^2)Cl[jchi](cvec[ii][[13]]
cvec[jj][[13]]q^2+cvec[ii][[12]]cvec[jj][[12]]),
{ii,2},{jj,2}];

ResCoeff[MJ,PhiPPJ]=Table[q^2/(4mN)Cl[jchi]cvec[ii][[11]]
(cvec[jj][[12]] - cvec[jj][[15]]q^2)+q^2/(mN)cvec[jj][[3]]
(cvec[ii][[1]]+cvec[ii][[2]](v^2-vmsq)),{ii,2},{jj,2}];

ResCoeff[SigmaPJ,DeltaJ]=Table[q^2/(4mN)Cl[jchi]
(cvec[ii][[4]]cvec[jj][[5]] - cvec[jj][[8]]cvec[ii][[9]]) -
q^2/(mN)cvec[jj][[2]]cvec[ii][[3]](v^2-vmsq),{ii,2},{jj,2}];

If[UseHelm==True,Sum[ResCoeff[MJ][[ii,jj]]*FF[DMmtx,MJ,J,T]
[[ii,jj]],{ii,2},{jj,2}],Sum[ResCoeff[MJ][[ii,jj]]*
FF[DMmtx,MJ,J,T][[ii,jj]]+ResCoeff[SigmaPPJ][[ii,jj]]*
FF[DMmtx,SigmaPPJ,J,T][[ii,jj]]+ResCoeff[SigmaPJ][[ii,jj]]*
FF[DMmtx,SigmaPJ,J,T][[ii,jj]]+ResCoeff[DeltaJ][[ii,jj]]*
FF[DMmtx,DeltaJ,J,T][[ii,jj]]+ResCoeff[PhiPPJ][[ii,jj]]*
FF[DMmtx,PhiPPJ,J,T][[ii,jj]]+ResCoeff[PhiTPJ][[ii,jj]]*
FF[DMmtx,PhiTPJ,J,T][[ii,jj]]+ResCoeff[MJ,PhiPPJ][[ii,jj]]*
FF[DMmtx,MJ,PhiPPJ,J,T][[ii,jj]]+ResCoeff[SigmaPJ,DeltaJ]
[[ii,jj]]*FF[DMmtx,SigmaPJ,DeltaJ,J,T][[ii,jj]],
{ii,2},{jj,2}]]
];
```

```
(*Function for computing the inelastic differential CS*)
DiffCrossSectionInel[ERkeV_,vv_]:=Block[{FFTemp,ER,bb,qq},

bb=bHO;
ER=ERkeV GeV;
qq=Sqrt[2M*(mN/GeV)*ERkeV] GeV;

FFTemp=If[M==1,
FFfinalInel[DensMatr,JIso,TIso]
/.q->qq/.y->((qq bb)/2)^2/.b->bb/.v->vv,
Exp[-2y]*FFfinalInel[DensMatr,JIso,TIso]
/.q->qq/.y->((qq bb)/2)^2/.b->bb/.v->vv
];

Return[M/(32Pi vv^2 mX^2 mN) FFTemp]/.FormalReplace//MyChop
];
```

```
(*Capture rate computation notebook*)
(*Import DARKSUSY+ClementzBlennow inputs and load package*)
nucZ = {0, 0, 1, 2, 2, 6, 7, 8, 10, 11, 12, 13, 14, 16,
18, 20, 26, 28};
nucA = {1, 1, 1, 4, 3, 12, 14, 16, 20, 23, 24, 27, 28,
32, 40, 40, 56, 58};
inData = Import["RadiusVescNumdens.txt", "Table"];
vEscData = inData[[All, {1, 2}]];
vEscInvData = inData[[All, {2, 1}]];
escape = Interpolation[vEscData];
escInv = Interpolation[vEscInvData];
suppressionData = Import["CleBlenSupp.txt", "Table"];
suppFac = Interploation[suppressionData];
<< "dmformfactor_sun.m";

(*Set DM and halo parameters and define units*)
Dits = 40;
MDDmin = -300`*^-6; MDDmax = 550`*^-6;
MDDstep = (MDDmax - MDDmin)/(Dits - 1);
MdList = Range[MDDmin, MDDmax, MDDstep ];
mX = 1000.;
MXJ = 1/2;
SetJChi[MXJ];
SetmX[mX];
SetDMSplit[mD];
vS = 220.0 kmPerS;
vG = 544.0 kmPerS;
vD = 270.0 kmPerS;
gFac = 1/(Erf[vG/vS] - 2/Sqrt[Pi]*vG/vS*Exp[-vG^2/vS^2]);
eta = Sqrt[3/2] vS/vD;
vO = eta*vS;
rhochi = 0.4 GeV/(cm^3)*GeV^(-4);
nDenschi = rhochi/mX;
bFM = "default";
rSun = Last[inData][[1]];
rStep = 3`*^6;
vMax = escape[0] kmPerS;
vMin = escape[rSun] kmPerS;
mN = 0.938272;
kg = 1/(1.79 *10^(-27));
cm = 10^(13) Femtometer*GeV;
GeVtoPerS = 1/(6.58*10^(-25 ));

(*Loop over all operators, skipping 2 since not included*)
For[op = 0, op < 15, op++;
```

```
If[op == 2, op = op + 1];
CapNoSupp = Table[0, {l, 16 + 1}, {k, Dits}];
Cap = Table[0, {l, 16 + 1}, {k, Dits}];

(*Loop over most abundant solar nuclei*)
For[nucNumb = 2, nucNumb < 18, nucNumb++;
 Z = nucZ[[nucNumb]];
 A = nucA[[nucNumb]];
 SetIsotope[Z, A, bFM, "default"];
 mT = A*mN;
 redM = mX*mT/(mX + mT);
 ZeroCoeffs[];
 SetCoeffsNonrel[op, 10^-3, 0];
 densData = inData[[All, {1, nucNumb}]];
 ndens = Interpolation[densData];

 (*Compute total CS with symbolic mass splitting*)
 Clear[mD];
 TotalCrossSection[u_, v_] := Block[{Energy1, a},
   a = GeV*
     Integrate[
      DiffCrossSectionInel[Energy1, Sqrt[u^2 + v^2]],
      {Energy1,
       xmin, xmax},
      Assumptions -> {(u^2 + v^2) >= 0,
      mD \[Element] Reals}];
   xmax = redM^2/mT (u^2 + v^2) (1 + Sqrt[1 -
      mD/(redM*(u^2 + v^2)/2)]) - redM/mT mD;
   kmin = redM^2/mT (u^2 + v^2) (1 - Sqrt[1 -
      mD/(redM*(u^2 + v^2)/2)]) - redM/mT mD;
   cmin = mX u^2/2 - mD;
   xmin = Max[cmin, kmin];
   Return[a*HeavisideTheta[xmax - cmin]];
   ];
 TotCross = TotalCrossSection[u, v];

 (*Capture rate functions based on section 2.3.1*)
 DifferCapt[v_, mX_, redM_, limlo_, limhi_] :=
  Block[{a, y, eta, Fu},
   eta = Sqrt[3/2] vS/vD;
   moving = Exp[-eta^2] Sinh[2 y eta]/(2 y eta);
   y = Sqrt[3/2] u/vD;
   Fu = Which[u >= (vG + vO), 0,
     u < (vG + vO) && u >= (vG - vO),
     3/(2 Sqrt[Pi] vD^2 eta) (u^2 + v^2)
      (Exp[-(u - vO)^2/vS^2] - Exp[-vG^2/vS^2]),
```

```
      u < (vG - vO), (3/2)^(3/2) * 4/Sqrt[Pi] * moving *
       u * (u^2 + v^2)*1/vD^3 * Exp[-3/2 u^2/vD^2]];
    a = NIntegrate[TotCross*Fu, {u, limlo, limhi},
      AccuracyGoal -> 5];
    Return[nDenschi*a];
    ];
  CaptRate[x_?NumericQ, mX_, redM_, limlo_?NumericQ,
    limhi_?NumericQ] := Block[{a},
    v = escape[x] kmPerS;
    a = DifferCapt[v, mX, redM, limlo, limhi]*4 Pi*
      (x*100 cm)^2*1/cm^3*ndens[x]*GeVtoPerS ;
    Return[a];
    ];

  (*Loop over mass splittings,
  compute capture rates as discussed in section 2.3.1*)
  For[j = 0, j < Dits, j++;
   mD = MdList[[j]];
   vLim = Re[Sqrt[2(mX mD - mD mT)/(mX mT)]];
   rLim = Which[vLim >= vMax, 0, vLim <= vMin, rSun,
      vMin < vLim < vMax, escInv[vLim/kmPerS]];
   imax = Floor[rLim/rStep];
   partSums = Table[0, {l, imax + 1}];

   (*Approximately compute the radial integral*)
   For[i = 0, i < imax, i++,
    x = i*rStep;
    v = escape[x] kmPerS;
    HiLim = Re[Sqrt[(2/(mX (mX - mT)^2)) (-mX mD mT +
       mD mT^2 + mX^2 mT v^2 + mX Sqrt[mX mT v^2
       (-2 mX mD + 2 mD mT + mX mT v^2)])];
    LoLim = Re[Sqrt[2 mD/redM - v^2]];
    partSums[[i]] = CaptRate[x, mX, redM, LoLim, HiLim];
    ];
   partialWidth = rLim/Length[partSums]*100 cm;
   CapNoSupp[[nucNumb - 2]][[j]] =
    gFac*Total[partSums]*partialWidth;
   CapNoSupp[[17]][[j]] += CapNoSupp[[nucNumb - 2]][[j]];
   Cap[[nucNumb - 2]][[j]] =
    gFac*Total[partSums]*partialWidth*suppFac[mD];
   Cap[[17]][[j]] += Cap[[nucNumb - 2]][[j]];
   ];
  ];
];
```